

Review

Recent Research Progress on Non-aqueous Lithium-Air Batteries from Argonne National Laboratory

Jun Lu * and Khalil Amine *

Chemical Sciences and Engineering Division, Argonne National Laboratory, 9700 South Cass Avenue, Lemont, IL 60439, USA

* Authors to whom correspondence should be addressed; E-Mails: junlu@anl.gov (J.L.); amine@anl.gov (K.A.).

Received: 6 October 2013; in revised form: 12 November 2013 / Accepted: 13 November 2013 /

Published: 18 November 2013

Abstract: Rechargeable non-aqueous Li-air battery technology offers potential advantages over other existing battery systems in terms of specific energy and energy density, which could enable the driving range of an electric vehicle to be comparable to that of gasoline vehicles. Development of efficient cathode catalysts and stable electrolytes for the Li-air battery has been intensively investigated for the past several years, and a number of review articles covering different topics are already available. This review mainly focuses on the research activities on rechargeable non-aqueous Li-air batteries at Argonne National Laboratory, with the emphasis on the gains in understanding of electrolyte decomposition, the structure and magnetic properties of lithium peroxide (Li_2O_2), development of an air-breathing cathode, and the effect of oxygen crossover on the lithium anode. Insights from this research have led to the improvement of the electrochemical performance of Li-air batteries. Promising paths for future work on rechargeable Li-air batteries are also discussed.

Keywords: Li-air battery; aprotic electrolyte; air-breathing cathode; oxygen crossover

1. Introduction

Development of advanced, reliable, and clean electrical storage devices would help to mitigate the diminishing fossil fuel supplies and environmental concerns regarding vehicles using conventional fuel. To address issues with global climate change, energy security, and energy sustainability, the electrification

of transportation and large-scale deployment of renewable energy have been considered an indispensable strategy [1]. However, such a transformation is severely limited by the unsatisfactory performance of current electrical energy storage systems. Although rechargeable lithium-ion batteries, one of the most promising electrical energy storage technologies available so far, are attractive owing to their high energy density and efficiency, they fall far below the requirement for electric vehicle (EV) and grid energy storage applications. For instance, the low energy storage capacity of state-of-the-art Li-ion batteries in EVs limits their driving distance to less than 100 miles per charge.

To make the transition from current hybrid electric vehicles (HEVs) to plug-in hybrid electric vehicles (PHEVs) or EVs, it is critical to develop a battery technology that enables acceptable driving ranges (300 miles per charge). This range requires much higher specific energy and energy density than those available from conventional Li-ion batteries. Therefore, researchers have been devoting an increasing amount of research on electrical energy storage systems that can go beyond the Li-ion battery limits [2–8].

Lithium-air cells can be considered the “holy grail” of lithium batteries because they offer, in principle, a significantly superior theoretical energy density compared to conventional lithium-ion systems, as shown in Table 1. For example, after electrochemical activation, layered lithium-manganese-nickel-cobalt-oxide cathodes, such as $\text{Li}_{1.200}\text{Mn}_{0.525}\text{Ni}_{0.175}\text{Co}_{0.100}\text{O}_2$, when coupled to a lithiated-graphite anode (LiC_6), can provide high capacity (~ 250 mA h/g) at an average open-circuit voltage of 3.6 V. This lithium-ion cell chemistry, the best to date, has a theoretical specific energy of ~ 900 W h/kg based on a calculation that uses the masses of the anode and cathode materials alone; in practice, 150–200 W h/kg has been accomplished at the cell level. In contrast, a Li-air cell, when discharged to the peroxide composition lithium peroxide (Li_2O_2) at an average voltage of ~ 3.0 V, would provide a theoretical specific energy of 3623 W h/kg, or when discharged to lithium oxide (Li_2O) at the same voltage, 5204 W h/kg. Note that gasoline (octane) offers a theoretical energy of $\sim 13,000$ W h/kg if the mass of the injected oxygen is not considered in the calculation because gasoline is supplied externally and combusted within, and exhausted from, the engine. By the same token, a Li-air cell would offer a specific energy of $\sim 11,000$ W h/kg if the “free” oxygen supplied during discharge and released during charge is ignored in the calculation.

Table 1. Relative specific energies of Li/O₂, lithium-ion and gasoline systems.

System	Reaction	Open circuit voltage (V)	Theoretical specific energy (W h/kg)
Li/O ₂ [8]	$2\text{Li} + \text{O}_2 \rightarrow 2\text{Li}_2\text{O}_2$	2.96	3,623 (incl. O)
	$4\text{Li} + \text{O}_2 \rightarrow 2\text{Li}_2\text{O}$	2.9	5,204 (incl. O)
	$4\text{Li} + \text{O}_2 \rightarrow 2\text{Li}_2\text{O}$	2.9	11,202 (excl. O)
Lithium-ion, e.g., C ₆ /LiMO ₂ (M = Mn, Ni, Co)	$\text{Li}_x\text{C}_6 + \text{Li}_{1-x}\text{MO}_2 \rightarrow \text{C}_6 + \text{LiMO}_2$	3.6	~ 900
Gasoline (octane)	$\text{C}_8\text{H}_{18} + 12.5\text{O}_2 \rightarrow 8\text{CO}_2 + 9\text{H}_2\text{O}$	-	$\sim 13,000$ (excl. O)

While the inherent energy potential of lithium metal approaches that of gasoline, today’s battery manufacturers have not yet been able to unlock this potential. While current lithium-ion batteries may provide acceptable power for HEVs and EVs, they do not provide sufficient energy for an acceptable

driving distance. This range limitation and the absence of a battery charging infrastructure have limited public interest in electric vehicles, particularly for long distance travel. A breakthrough in Li-air battery technology would significantly increase the possibility of extending the electric range of these vehicles, with the added advantages of reducing battery cost and weight. Recently, the enormous potential that the Li-air battery possesses triggered sharply increased research activity, as evidenced by over 300 research articles, including about 20 review articles, having been published on this technology in the last four years alone. In 2009, Argonne National Laboratory launched a project with the main goal of developing innovative and radically new concepts that will dramatically advance Li-air batteries with an energy density far surpassing that of conventional lithium-ion batteries, achieving the requirement for electrically powered vehicles. Under this project, a multidisciplinary team was established from a broad spectrum of basic and applied scientific disciplines with additional advantages of using Argonne's unique research facilities. The team worked closely together to develop a Li-air battery system with exceptionally high energy density and charge-discharge reversibility by pursuing new approaches that combine innovation in advanced electrode-, electrolyte-, and catalytic materials research, assisted by extensive computer modeling and advanced characterization techniques.

In this short review article, except for a brief overview of Li-air batteries (Section 2), we will mainly focus on the research activities with regard to non-aqueous Li-air batteries from Argonne under the above-mentioned project [9–34]. The following sections cover the stability of the electrolyte and its influence on the electrochemical performance of Li-air cells, the structure and magnetic properties of Li_2O_2 and its relevance to the Li-air battery design, the design and optimization of the air cathode structure with different types of catalyst, the oxygen cross-over effect on the Li anode based on both experimental and theoretical modeling results, and the development of a single-crystal silicon membrane with high lithium conductivity. The last section of the article will discuss future challenges with the aim to gain a better understanding of this promising battery technology. Covering the immense body of work published in this field is beyond the scope of the article. For those who are interested, more detail of recent research progress and fundamental understanding from other research groups can be found in many review articles [3,5,8,29,35–51] (and the references cited thereby) published in the last few years.

2. Concept and Challenges for Li-Air Batteries

The Li-air battery chemistry uses the oxidation of lithium at the anode and reduction of oxygen at the cathode to induce current flow. Originally proposed in the 1970s as a possible power source for electric vehicles, Li-air batteries recaptured scientific interest in the late 2000s due to advances in materials technology and an increasing demand for environmentally safe and oil-independent energy sources [2,7,52–62]. Because oxygen is supplied as a gaseous reactant to the cell during discharge, Li-air cells differ from conventional battery systems such as lead-acid, nickel-metal hydride, and lithium-ion; they can be constructed as part of hybrid battery-fuel cell systems. Compared to other metal-air batteries such as Zn-air and Al-air cells, which have aqueous electrolytes and operate at a relatively low voltage of ~ 1.4 V and ~ 1.2 V, respectively, non-aqueous Li-air cells provide ~ 3 V and, therefore, a significantly higher specific energy [63]. During electrochemical discharge, the lithium anode is oxidized by releasing electrons to the external circuit to produce lithium ions in the electrolyte,

whereas the oxygen is reduced at the catalytic cathode surface to form, in the case of non-aqueous electrolytes, Li_2O_2 or Li_2O [51]. In addition, because the Zn-air and Al-air electrochemical reactions are not readily reversible, these metal-air cells have to be mechanically recharged with fresh anodes and electrolytes. In contrast, non-aqueous Li-air cells can be recharged internally, particularly when the discharge is restricted to the formation of Li_2O_2 .

There are two principal electrochemical reactions of interest in non-aqueous Li-air batteries:



Theoretically, the full reduction of O_2 to Li_2O [Equation (2)] is desired because of its higher specific energy and energy density. However, this reaction involves a four-electron transfer, which is not favored for substrates with weak binding for oxygen, such as carbon, the most widely used cathode material in the Li-air battery. If the cut-off voltage is lowered to 2.0 V or below (vs. Li/Li^+), Li_2O does appear to be the main discharge product on the cathode, but the subsequent charge of Li_2O , the reverse reaction in Equation (2), cannot proceed under the test condition due to the thermal stability of Li_2O [64]. Therefore, Li_2O_2 is the reaction product observed in most recent cell tests (cut-off voltage >2.0 V). From a kinetic point of view, the formation of Li_2O_2 during discharge may be beneficial to the rate performance of the cell, since full cleavage of the O–O bond may not be necessary if a suitable catalyst can be identified. During charge, Li_2O_2 can decompose via either a two-electron process, $\text{Li}_2\text{O}_2 \rightarrow 2\text{Li}^+ + 2\text{e}^- + \text{O}_2$, or a one-electron process that involves the formation of lithium superoxide (LiO_2), $\text{Li}_2\text{O}_2 \rightarrow \text{Li}^+ + \text{e}^- + \text{LiO}_2$; these processes permit rechargeability of the non-aqueous Li-air cell. However, the reactivity of the other components of the Li- O_2 cells, including the electrolyte, electrocatalysts, carbon support, and lithium anode has a significant impact on the oxygen reduction reaction on discharge and oxygen evolution reaction on charge and thus on the overall cell performance [12,55,56,65], as will be detailed in the following sections.

The successful development of non-aqueous Li-air cells has been hampered because of severe materials and technological problems that have limited electrochemical performance: (1) the non-aqueous electrolytes are unstable during the discharge due to presence of reduced oxygen species; at high potential during charge, they are easily oxidized by the oxygen released; thereby seriously limiting cycle life; (2) during discharge, the solid and insoluble Li_2O_2 products are deposited on the surface or within the pores of the carbon cathode, thereby clogging the pores and restricting oxygen flow; (3) poisoning of the lithium electrode due to oxygen crossover occurs and destroys the integrity and functioning of the cell; and (4) commonly used cathode catalysts, such as MnO_2 or Mn metal, do not access the full capacity of the oxygen electrode or enable sufficiently high rates.

3. Effect of Organic Electrolytes

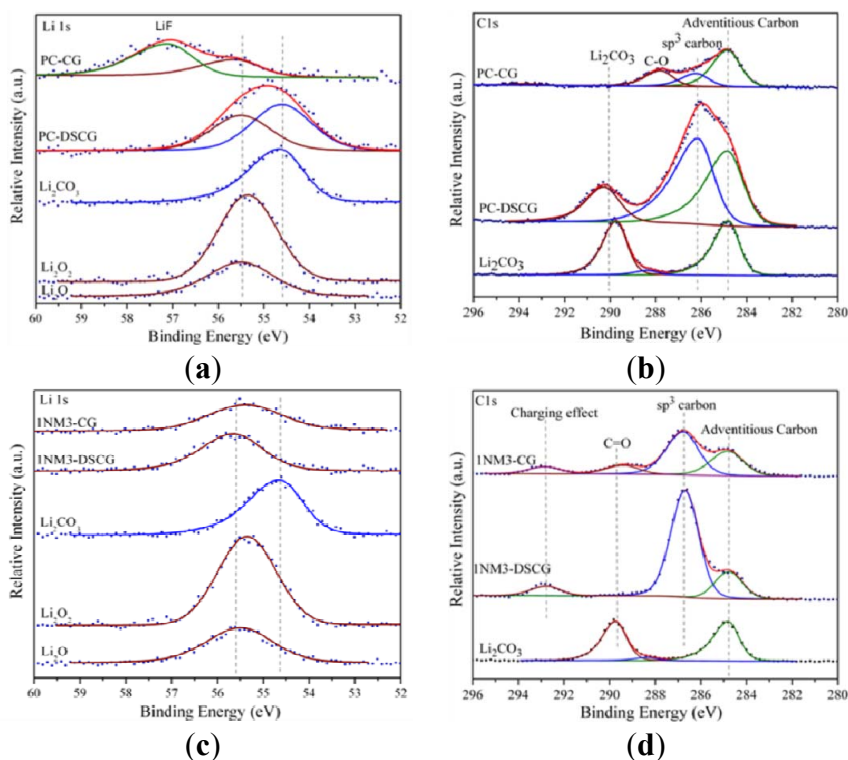
Recently, it has been recognized that the choice of the electrolyte, in particular, the organic solvent, might be the most critical factor in the development of rechargeable non-aqueous Li-air cells [36,40]. A good electrolyte should be able to survive from the nucleophilic attack of the superoxide radical (O_2^-), which is believed to be the intermediate phase formed from the oxygen reduction reaction upon discharge. Reaction with such highly reactive species (LiO_2 , O_2^-) to form decomposition products is especially

problematic for carbonated-based electrolytes, as will be detailed below. In addition to its stability against superoxide radical, a good electrolyte for Li-air cells should also meet the following criteria: a wide potential window to withstand high oxidation potentials; stable toward reaction with the lithium anode; low viscosity and volatility; and high oxygen solubility and diffusivity [66]. Ideally, the electrolyte should be able to dissolve the discharge products, *i.e.*, Li_2O_2 , at least partially. Unfortunately, none of the electrolytes investigated so far for Li-air cells meets all of the above requirements, despite significant efforts to that end in the past few years. Understanding the reaction mechanisms between the electrolytes and discharge products will, no doubt, be the key to developing a stable electrolyte for Li-air cells.

A wealth of experimental and theoretical evidence indicates that the organic carbonates [e.g., propylene carbonate (PC), ethylene carbonate, and dimethyl carbonate] commonly used in Li-ion batteries are not stable toward the oxygen reduction products formed during battery discharge [64]. During discharge, in addition to formation of the desired Li_2O_2 , PC decomposes, resulting in the formation of lithium carbonate (Li_2CO_3) and other organic species [67]. Another challenge besides the decomposition of the electrolyte is the large overpotential observed in the Li-air cell, which affects both power and cycle life [5].

To understand the source of the large polarization observed in the Li-air cell, Zhang *et al.* [27] carried out a detailed investigation of the charge and discharge products formed in cell systems employing the PC-based electrolyte. They employed X-ray photoelectron spectroscopy (XPS) as a primary tool to characterize the charge and discharge products, as shown by the spectra in Figure 1.

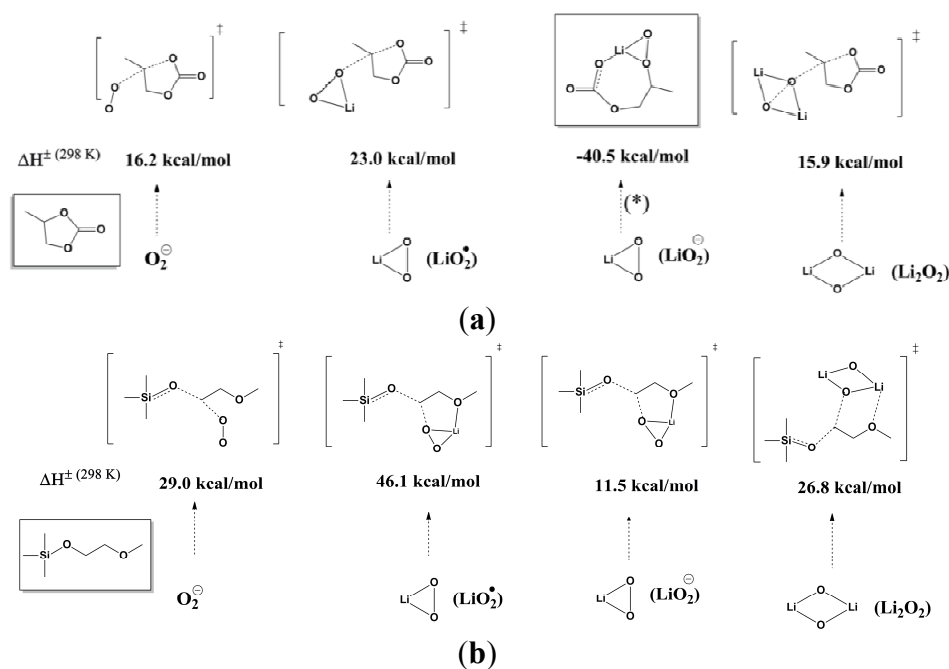
Figure 1. X-ray photoelectron spectroscopy (XPS) spectra of Li 1s and C 1s core peaks of the cathode carbon electrodes after discharge and charge: (a) Li 1s and (b) C 1s in propylene carbonate (PC); and (c) Li 1s and (d) C 1s in tri(ethylene glycol)-substituted methyltrimethyl silane (1NM3). Standard compounds Li_2O_2 , Li_2O and Li_2CO_3 are listed at the bottom of each spectrum. Reprinted with permission [27]; Copyright 2011, American Chemical Society.



The results indicated that Li_2CO_3 was the major product formed during discharge, with only minor amounts of lithium oxides being formed. The XPS data also indicate that, during the first charge cycle the Li_2CO_3 was decomposed. This reaction is believed to be the primary cause of the large overpotential required for charging, owing to the need to oxidize the carbonate or other materials rather than the desired Li_2O_2 .

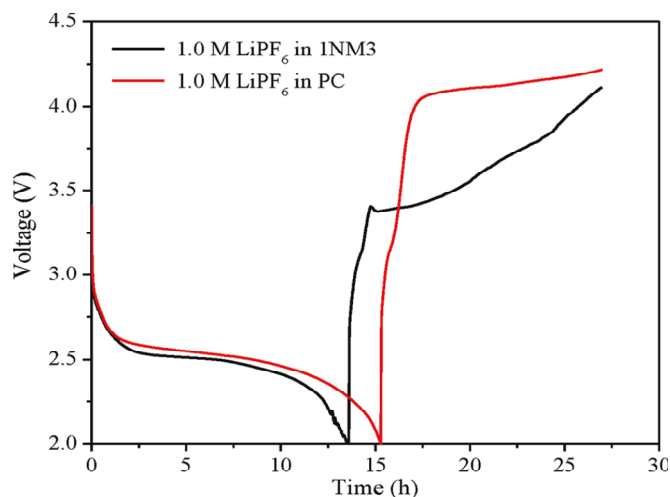
Zhang *et al.* [27] also employed a density functional theory (DFT) and high level quantum chemistry calculation to address the decomposition of PC in the Li-air cell during discharge. They considered four possible intermediates from the oxygen reduction reaction of O_2 , *i.e.*, O^{2-} , O_2^{2-} (Li_2O_2), LiO_2 and LiO_2^- . The modeling results showed that “ring-opening”, *i.e.*, C–O bond breaking of PC, is the first step in the decomposition of PC to Li_2CO_3 or other lithium alkyl carbonates; this observation is consistent with the findings of Bryantsev *et al.* [68] The calculated energy barriers for all four species are quite small, with LiO_2^- being the most reactive, as shown in Figure 2a. The energy barrier for the subsequent C–O bond breaking is relatively smaller than the first step; therefore, it is thermodynamically favorable. In other words, upon “ring-opening” of PC, the following reactions are thermodynamically downhill, which could lead to the formation of Li_2CO_3 and other products such as formaldehyde and acetaldehyde with the assumption that a second electron transfer can occur. The DFT calculations confirmed that PC is unstable to oxygen reduction species. At present, Li-air cells based upon PC cannot be considered viable as the overall reaction appears to be oxidation of PC to CO_2 . The PC decomposition during the discharge has also been reported by other groups [65,67].

Figure 2. Comparison of the computed barriers (enthalpies) for activation of (a) PC decomposition by O_2 anion radical (O_2^-), Li_2O radical, Li_2O anion (LiO_2^-), and Li_2O_2 ; and (b) (ethylene glycol)-substituted methyltrimethyl silane (1NM1) decomposition by O_2 anion radical, Li_2O radical, Li_2O anion, and Li_2O_2 . The reaction of Li_2O anion with PC is exothermic by 40.5 kcal/mol and is a barrierless process. The O_2 anion radical barriers at G4MP2 are 12.1 kcal/mol (for PC) and 21.4 kcal/mol (for 1NM3). Reprinted with permission [27]; Copyright 2011, American Chemical Society.



To identify more stable electrolytes that do not generate side reactions during the discharge, Zhang *et al.* [27] investigated the reactivity of a new silicon-containing oligo(ethylene oxide) solvent, tri(ethylene glycol)-substituted methyltrimethyl silane (1NM3). The DFT calculations indicated that this new solvent seems to be more stable to the highly active oxygen reduction species when compared to PC, as shown in Figure 2b. When 1NM3 is used in place of PC in a Li-air cell, the XPS data collected after a single discharge show that only lithium oxides are formed; moreover, they are partially decomposed upon charging (Figure 1c). The increased stability of the 1NM3 solvent results in a significantly lower overpotential for the Li-air cell, as shown in Figure 3. The finding that the product from charging in the 1NM3 is oxygen needs confirmation, but the lower overpotential could be due the oxidation of lithium oxides being easier than the oxidation of the carbonate that is formed in the PC-electrolyte cells. Clearly, the electrolyte solvent stability plays a key role in the performance of Li-air batteries and will be a factor in improving their efficiencies. While the stability during discharge found for the 1NM3 electrolyte is an encouraging result for Li-air cell development, electrolytes that provide stability during charge are also needed to aid in reversibility of the reactions. Note that the reversibility and cycling stability of 1NM3-based Li-air cells were still not satisfactory, which might be attributed to the failure caused by decomposition of the lithium oxides on charge, since some of the lithium oxides might require a higher potential for decomposition.

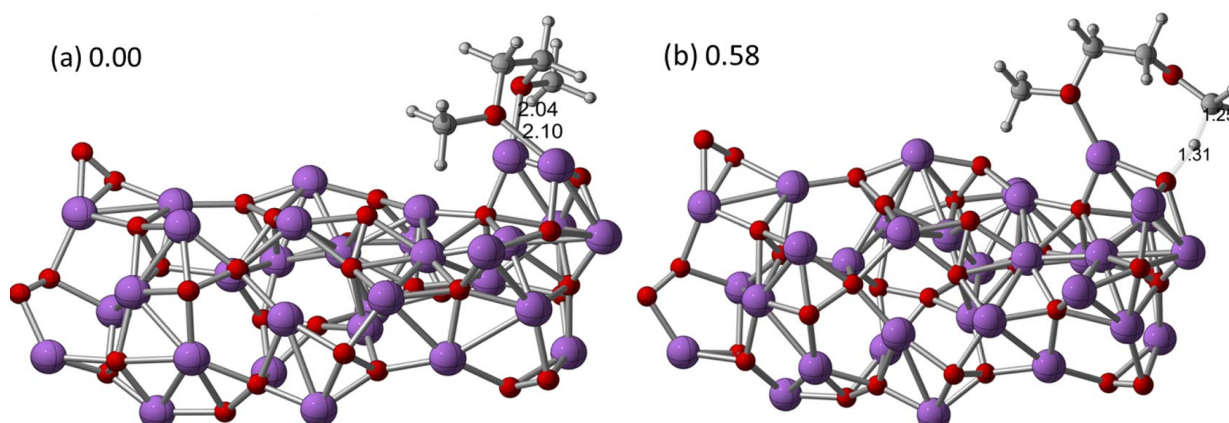
Figure 3. First charge and discharge cycles of a Li-air cell with PC and 1NM3. Reprinted with permission [27]; Copyright 2011, American Chemical Society.



The reactions of the electrolyte at the lithium oxide/peroxide surfaces (the discharge products in a Li-air cell) could also be responsible for the degradation of the solvent, in addition to the O_2^- that has been postulated to be present in the electrolyte. Recent DFT calculation results on the interactions of dimethoxyethane (DME) with Li_2O_2 clusters indeed demonstrated a high possibility of such reactions [22]. In this work, small Li_2O_2 cluster models of up to 16 Li_2O_2 units were used to represent possible surface sites on the Li_2O_2 discharge products to investigate the reactions with ether, as shown in Figure 4. The computations indicated that hydrogen abstraction by an unpaired spin on a Li–O–Li site (if present on the surface) may be favorable for decomposition of DME, which likely leads to the formation of reactive radicals and, subsequently, in the presence of oxygen, can lead to oxidized species such as aldehydes and carboxylates as well as LiOH on the surface of the Li_2O_2 . In contrast, the decomposition

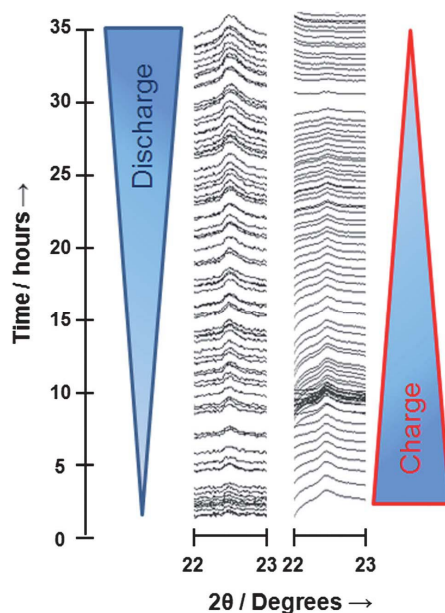
initiated by the proton abstraction from the secondary position of DME by the singlet cluster (O–O site) results in an endothermic product, and subsequent reactions require the presence of oxygen or superoxide to be exothermic. Thus, pathways involving proton abstraction are less likely than those involving hydrogen abstraction. These results suggest that, if Li–O–Li sites with spin exist on a Li₂O₂ surface, they could be detrimental to Li-air cells by providing energetically favorable chemical mechanisms for DME decomposition at the Li₂O₂-electrolyte interface during discharge or charge. It is reasonable to expect that the hydrogen abstraction mechanism would also likely occur for other longer chain ether solvents as well, such as tetraethylene glycol dimethyl ether (TEGDME), one of the most widely used solvents in Li-air cells recently.

Figure 4. Optimized structures for the (a) (Li₂O₂)₁₆-dimethoxyethane (DME) cluster (quintet) and (b) transition state structure for the abstraction of a primary hydrogen from the DME at the B3LYP/6-31G (d) level of theory. Selected bond distances (Å) and relative energies (eV) were also shown. Reprinted with permission [22]; Copyright 2013, American Chemical Society.



Ryan *et al.* [26] experimentally investigated the stability of ether-based electrolytes in a Li-air cell by a combined electrochemical and spectroscopic (FT-IR) measurement. In particular, they attempted to identify electrolyte decomposition species that may remain soluble in the electrolyte, if any. Through well-controlled experiments, they drew the conclusion that the electrochemical stability of the ether-based solvents may not be as great as previously considered. They found that ethers, for instance, 1NM3 or TEGDME, are consumed as part of the charging process in working Li-air cells, even under moderate voltages in the absence of O₂, which is consistent with the theoretical calculations discussed above. In another study on the stability of TEGDME electrolyte using *in-situ* synchrotron X-ray diffraction (XRD), Ryan *et al.* [20] found the reversible formation of Li₂O₂ upon discharge and charge, as shown in Figure 5. Through the Rietveld refinement of the discharge data on the Li₂O₂ (100), (101), and (110) reflections, they also reported a general trend of increasing grain size of Li₂O₂ from 10 nm to 120 nm as the discharge progresses. However, if an identical cell is allowed to charge first to force some of the electrolyte to decompose prior to the discharge, Ryan *et al.* [20] observed the reversible formation of LiOH rather than Li₂O₂ on the following cycle test. This surprising result may indicate that electrolyte decomposition can completely alter the nature of the stable discharge products in the Li-air cell.

Figure 5. Three-dimensional line plot for the (110) reflection of Li_2O_2 which shows complete reversibility on discharge and subsequent charge. Reprinted with permission [20]; Copyright 2013, Royal Society of Chemistry.



As a consequence of the electrolyte decomposition, the byproducts (insoluble lithium precipitates) from these side reactions will accumulate on the cathode, which not only blocks the oxygen diffusion, but also increases the cathode impedance. Whether the failed cathode was permanently damaged or recoverable, a repairable cathode suggests that the battery life could be dramatically extended if a more stable electrolyte were used. In an attempt to address this issue, Shui *et al.* [15] investigated the cathode's failure and recoverability of the Li-air cell and inferred that passivation by insoluble lithium precipitates from the electrolyte decomposition was responsible for the cathode failure. The spent cathode could nearly return to its original performance upon removal of the precipitates (mainly lithium carbonate) by acidic treatment, which is attributed to the recovery of the porous structure of the cathode, as confirmed by scanning electron microscopy (SEM) images (Figure 6). This study indicated that the lifespan of the Li-air battery could be extended, in principle, if the passivation layer were removed in a timely manner.

Shui *et al.* [14,18] also investigated the distribution of insoluble lithium precipitates in the separator region of non-aqueous Li-air batteries, using microfocused synchrotron X-ray diffraction (μ -XRD). They reported that, unexpectedly, a significantly higher concentration of precipitates was found in the separator region than in the cathode. The μ -XRD results showed that these precipitates are mainly crystallized Li_2CO_3 , which grew on the separator fiber surface, as revealed in the SEM images in Figure 7. Under severe electrolyte decomposition, such precipitate formation could lead to the blockage of the pores in the middle layer of the separator, thereby constricting the electrolyte-mediated ion transport. Moreover, these precipitates in the separator are electrochemically non-decomposable, since the separator is insulated from the electrochemical reactions, resulting in higher observed accumulation at the separator.

Figure 6. Scanning electron microscopy (SEM) images of the cathode surface of: (a) a fresh cathode, (b) a used cathode from a failed cell after multi cycles, (c) the used cathode after being washed in 0.5 M H₂SO₄ for 10 min; and (d) X-ray diffraction (XRD) patterns of cathodes shown by (a), (b) and (c) with reference Li₂CO₃. Reprinted with permission [15]; Copyright 2013, Elsevier.

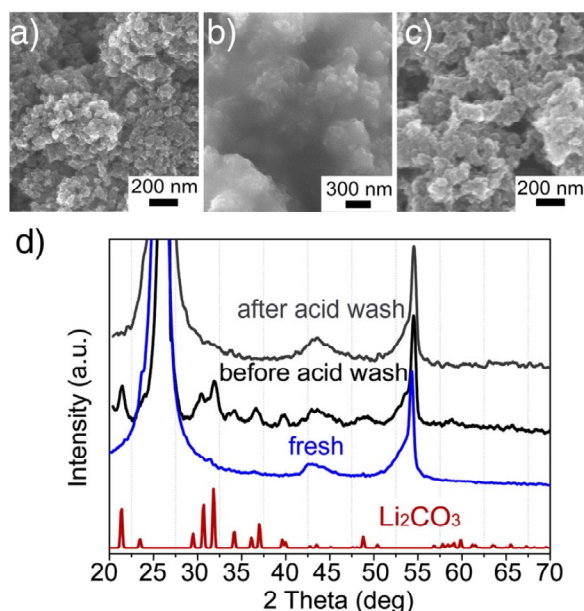
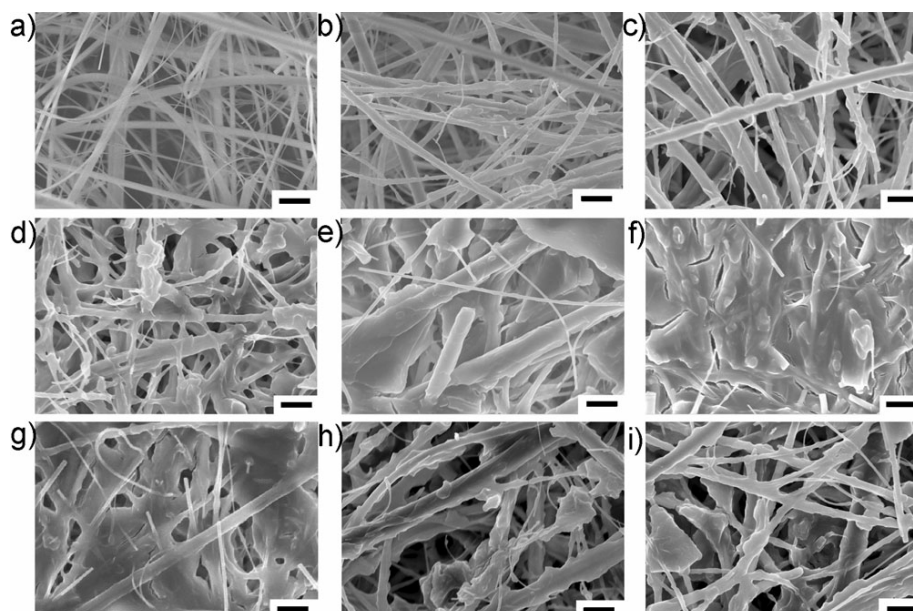


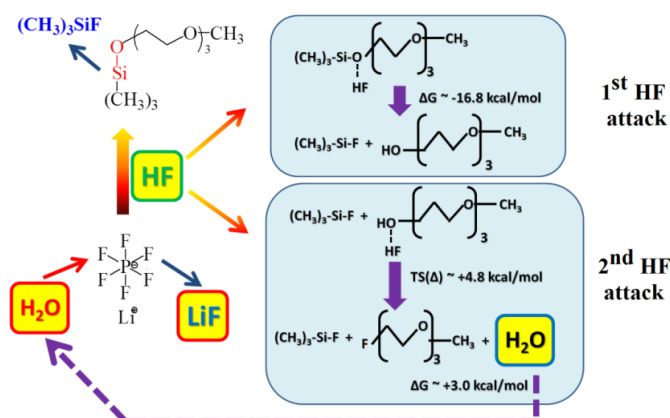
Figure 7. SEM images of (a) fresh separator and (b–i) separator slices from a failed battery sampled at equal distances from the cathode to the anode. The scale bar is 2 μ m. Reprinted with permission [14]; Copyright 2012, Wiley-VCH Verlag GmbH & Co. KGaA, Weinheim.



Besides the stability of solvents, another source of detrimental electrolyte decomposition in Li-air batteries could be from side reactions due to the decomposition of lithium salt used in the electrolytes. The stability of lithium salt, especially in the presence of reduced oxygen species (O₂⁻) and trace amount of H₂O, may significantly affect the cyclability and capacity of Li-air cells. Moreover, these

side reactions, if they are not electrochemical reactions, will not be evident on the voltage/capacity profiles and, therefore, will be difficult to investigate. Applying a combined experimental and computational approach, Du *et al.* [32] provided evidence that the stability of the electrolyte used in the Li-air cell strongly depends on the compatibility of the lithium salt with the solvent. In the case of the LiPF₆-1NM3 electrolyte, the decomposition of LiPF₆ occurs in the cell, as evidenced by *in-situ* XRD, FT-IR, and XPS analyses. This decomposition forms HF and triggers the decomposition of the 1NM3 solvent. Figure 8 shows a possible mechanism for the decomposition of the 1NM3-LiPF₆ electrolyte observed experimentally, which was further confirmed by *ab initio* molecular dynamics simulations of the bulk 1NM3-LiPF₆ electrolyte. These reactions lead to degradation of the electrolyte and cause the poor cyclability of the cell. The same reactions are not observed when lithium bis(trifluoromethanesulfonyl)imide (LiTFSI) and LiCF₃SO₃ are used as the lithium salt in 1NM3 solvent, or when LiPF₆ is used in TEGDME solvent, suggesting that the stability of the electrolyte in Li-air cells depends on the compatibility of lithium salt with solvent.

Figure 8. Schematic reaction mechanism for decomposition of LiPF₆-1NM3 electrolyte in the Li-O₂ cell. Reproduced from [32] with permission from the PCCP Owner Societies.



4. Structure and Magnetic Properties of Li₂O₂ and Relevance to Lithium-Air Battery

Better understanding of the electronic and structural properties of lithium oxides (Li_xO_y) could help us elucidate the charge and discharge chemistries involved in the Li-air battery. Unfortunately, the Li-O₂ phase diagram remains elusive and far from complete. In general, the most commonly known stoichiometric Li_xO_y compounds with a thermodynamically stable structure in condensed phase are Li₂O (lithia) and Li₂O₂ [25]. Similar to Li₂O, crystalline bulk Li₂O₂ is known from theoretical predictions to be a semiconductor with an electronic band gap of ~ 4.9 eV [69–71]. Such high band gap fails to explain the electronic conductivity and charge transfer required for the redox chemistry in an operating Li-air cell cathode. To address this issue, Hummelshoj *et al.* [69,72] recently proposed a theory based on metallicity in bulk Li₂O₂ induced by Li vacancies, whose formation energy is predicted to be ~ 3.0 eV and depends on the vacancy concentration. The theory is supported by the finding that the Li₂O₂ observed as the discharge product of a Li-air cell is generally in the form of nanoparticles [71,73].

The mechanism of the formation and growth of Li₂O₂ products in Li-air batteries during discharge is currently not well understood, nor is the mechanism of the decomposition of Li₂O₂ during charge.

Therefore, computational studies are needed to investigate the structural and electronic properties of small Li_2O_2 clusters, considering that computations on large clusters or particles would be much more complicated and costly. The information gathered from theoretical computations could provide insight into the nucleation of Li_2O_2 during battery discharge as well as the properties of larger nanoparticles. In a recent article, Lau and co-workers [24] reported on a DFT study of the structure of $(\text{Li}_2\text{O}_2)_n$ clusters ($n = 1-4$). Many possible structures of the clusters and the corresponding electronic states were considered in their calculations, as shown in Table 2. High-level G4 theory calculations showed, surprisingly, that the triplet state is significantly stabilized relative to the singlet in these clusters, especially for clusters larger than the dimer. The DFT calculations also showed that a cluster with $n = 16$ has a high spin state, which can be characterized by O–O pairs protruding from the surface but still chemically bonded to the Li of the clusters. The distinct O–O pairs found on the high spin stoichiometric Li_2O_2 clusters suggest the existence of superoxide-like surface structures, considering the short O–O distances and a localized unpaired spin on the surface compared to a peroxide pair as found in a Li_2O_2 bulk crystal, which has longer O–O distance and no spin. These superoxide-like surface structures, if they indeed exist experimentally, could have important implications for the electrochemistry of formation and decomposition of Li_2O_2 in Li-air batteries, including surface electronic conductivity and electrolyte surface reactions.

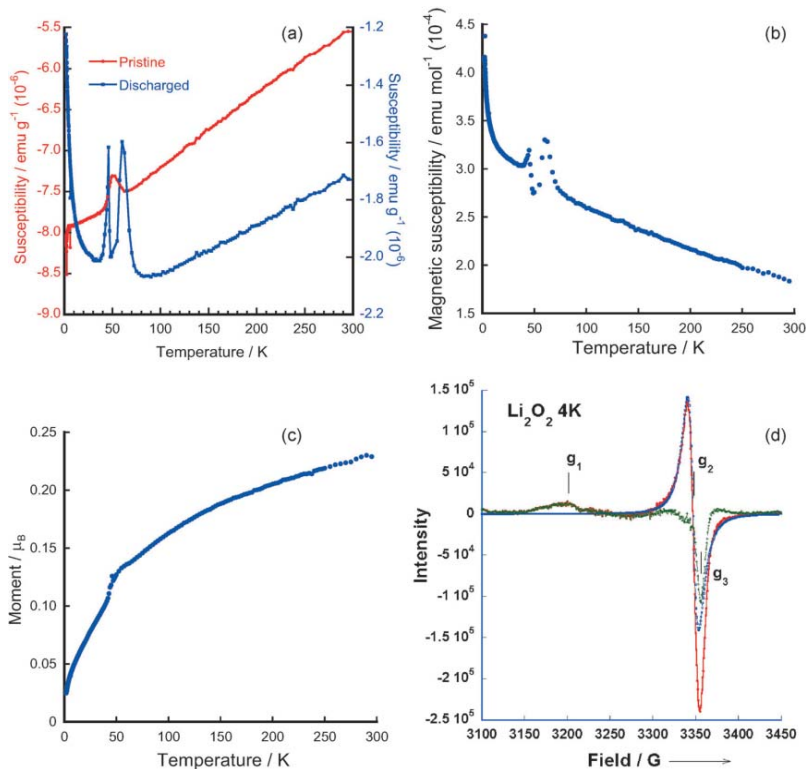
Table 2. Energies of triplet state relative to singlet state (in eV) of $(\text{Li}_2\text{O}_2)_n$ Clusters, $n = 1-4$, at various levels of theory; also given in the Table is the energy of the quintet state relative to the singlet for the $(\text{Li}_2\text{O}_2)_{16}$ cluster. Reprinted with permission [24]; Copyright 2012, American Chemical Society.

N	State ^a	B3LYP/6-31G(2df)// B3LYP/6-31G(2df)		PBE/PW//PBE/PW ^b	G4 theory	
		E_e	G_{298}	E_e	E_e	G_{298}
1	singlet (1)	0.00	0.0	0.0	0.0	0.0
	triplet (1)	0.96	0.86	0.88	1.27	1.17
2	singlet (4)	0.0	0.0	0.0	0.0	0.0
	triplet (4)	−0.04	−0.21	−0.02	0.55	0.36
3	singlet (11)	0.0	0.0	0.0	0.0	0.0
	triplet (11)	−0.48	−0.72	−0.49	−0.08	−0.32
4	singlet (22)	0.0	0.0	0.0	0.0 ^c	0.0 ^c
	triplet (22)	−0.45	−0.64	−0.55		
16	singlet (1)	0.0 ^d	0.0 ^d	0.0	−0.17 ^c	−0.35 ^c
	quintet (1)	−1.09 ^d	−1.39 ^d	−1.03		

^a: The number of structures investigated for each state is given in parentheses. In some cases, these structures were investigated at the B3LYP/6-31G* level, and only the most stable were refined at the larger basis set level. The initial guess for the triplet state was usually the singlet state geometry; ^b: Perdew-Burke-Ernzerhof (PBE) functional with plane wave (PW) basis set (see text); ^c: G4MP2 theory; ^d: B3LYP/6-31G(d)//B3LYP/6-31G(d) level of theory. The unrestricted triplet converges to the quintet due to spin contamination. There is no significant spin contamination present in the triplet states of the smaller clusters ($n = 1-4$), which were done using unrestricted B3LYP wave functions.

Inspired by the above computational study, Lu *et al.* [13] recently investigated the magnetic properties of the Li_2O_2 discharge products formed in an ether (1NM3)-based electrolyte, which lead to a better understanding on preparing successful Li-air batteries. Using electron paramagnetic resonance (EPR) and superconducting quantum interference device (SQUID) magnetometry, they found evidence for paramagnetism in the Li_2O_2 discharge product, as shown in Figure 9. The EPR spectra, by comparison to the EPR spectra of LiO_2 from the literature, also provided direct evidence that the spin in the discharge Li_2O_2 product is caused by a superoxide-type structure. This finding confirmed the DFT calculations that superoxide-type surface oxygen groups with unpaired electrons exist on some stoichiometric Li_2O_2 nanoparticle surfaces. In addition, the number of spins predicted by using DFT is approximately consistent with the magnetic measurements of the discharged Li_2O_2 product.

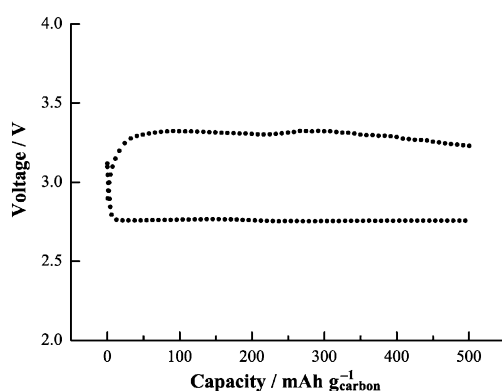
Figure 9. Magnetic susceptibility data from superconducting quantum interference device (SQUID) measurements for: (a) pristine carbon cathode before cycling and discharged cathode with 1NM3- LiCF_3SO_3 electrolyte; (b) difference between pristine carbon cathode and initially discharged cathode; (c) magnetic moment data from SQUID measurement for Li_2O_2 bulk powder; and (d) electron paramagnetic resonance (EPR) spectrum of Li_2O_2 bulk powder at 4 K. The red trace is the experimental result. The blue trace is the calculated one line Lorentzian spectrum to fit the central peak at g_2 value; and the green trace is the difference between red and blue traces to reveal peaks at g_1 and g_3 . Reprinted with permission [13]; Copyright 2013, Wiley-VCH Verlag GmbH & Co. KGaA, Weinheim.



The presence of magnetism in the Li_2O_2 discharge product could play an important role in the charge and discharge chemistries of Li-air batteries, since the superoxide-type surface oxygen groups with spin could enable the electronic conductivity mechanism that is required for the reversible formation and decomposition of Li_2O_2 . As consequence, Li-air cells with such discharge products

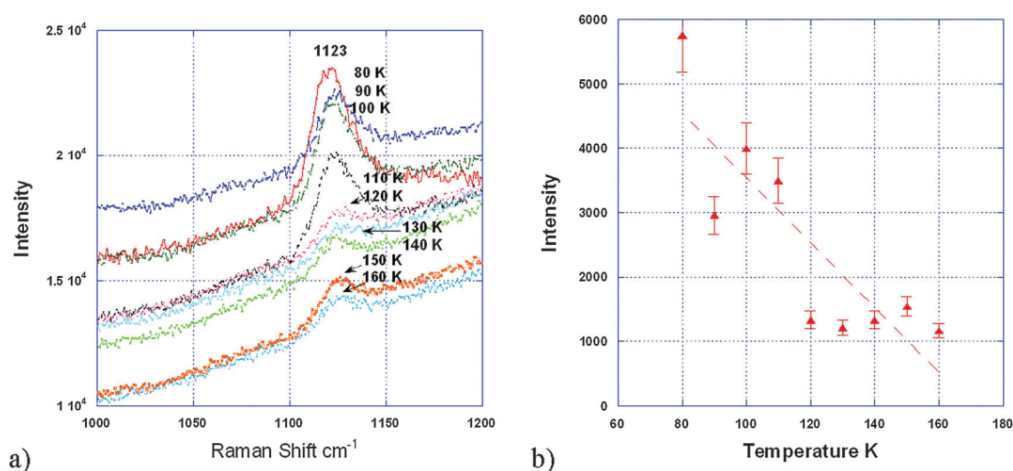
achieved a low charge potential (3.3 V), as shown in Figure 10. The presence of spin, as found in the experiments and as suggested to be present on the Li_2O_2 surface in the calculations, provides a possible mechanism for the electronic conductivity for the reversible electrochemical formation and decomposition of Li_2O_2 [13]. The calculated DFT density of states from the “superoxide” species for the high spin state of a Li_2O_2 surface indicates the presence of a finite density of states in the band gap. Analysis of the density of states indicates that these states come from the surface superoxide species, which could give rise to surface electrical conductivity. Thus, electrochemical decomposition and formation of Li_2O_2 could be enabled by this surface conductivity, as well as effective connectivity through grain boundaries between nanoparticles and interfaces with the carbon.

Figure 10. Voltage profile during first discharge-charge of Li-O₂ cell based on the 1NM3-LiCF₃SO₃ electrolyte. Reprinted with permission [13]; Copyright 2013, Wiley-VCH Verlag GmbH & Co. KGaA, Weinheim.



Recent work by Yang and co-workers [33] further confirmed the presence of a LiO_2 -like species in the Li_2O_2 discharge product by the presence of a peak at 1125 cm^{-1} in the Raman spectra (Figure 11), in addition to the peaks expected for Li_2O_2 .

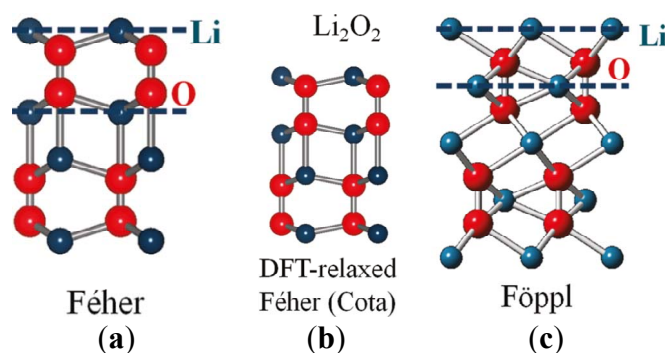
Figure 11. (a) Raman spectra of the discharged activated carbon (AC) surface between 160 K and 80 K showing that the superoxide peak $\sim 1125\text{ cm}^{-1}$ increases with decreasing temperature; (b) superoxide peak intensity estimated from its peak height between 160 K and 80 K. The dash line is a guide for the eyes. Reproduced from [33] with permission from the PCCP Owner Societies.



In this work, they applied a petroleum coke-based activated carbon (AC) as cathode material and a TEGDME-LiCF₃SO₃ electrolyte to investigate the discharge/charge behavior of a Li-air cell. Electrochemical measurement surprisingly showed two distinct voltage plateaus during charging, at 3.2–3.5 V and 4.2–4.3 V vs. Li⁺/Li, where the lower plateau corresponds to a form of Li₂O₂ with superoxide-like properties characterized by a low temperature magnetic phase transition (49.7 K) and a high O–O stretching frequency (1125 cm⁻¹). Yang *et al.* [33] also observed that the magnetic phase transition and the high O–O stretching frequency disappear when the cell is charged to above 3.7 V. This finding suggests that a superoxide surface species with a low-temperature phase transition results in a lower charge potential, and control of the forms of Li₂O₂ produced on discharge is important for improving the efficiency of Li-air batteries.

In addition to the electronic and magnetic properties, the crystalline structure of Li₂O₂ is also of vital importance to the study of Li-air batteries. In the 1950s, two disparate crystal structures were proposed for Li₂O₂ from XRD studies, the Féher [74] and Föppl [75] structures, which have different lithium sublattices, as shown in Figure 12. Along the *c*-lattice direction, Féher's original structure consists of lithium and oxygen atoms nominally sharing each plane, whereas Föppl's revised structure positions of the lithium sites between adjacent oxygen planes. Although these two structures share similar nearest-neighbor Li–O distances (1.91 Å in Féher's vs. 1.98 Å in Föppl's), the O–O bond distances are dramatically different (1.28 and 1.55 Å, respectively). To assess these competing Li₂O₂ structures, Chan *et al.* [28] recently employed a combination of high-energy XRD and nonresonant inelastic X-ray scattering (NIXS) spectra with first-principle calculations using the Bethe-Salpeter Equation. Their data indicated that Föppl's structure is more appropriate for Li₂O₂. The measured and computed spectra and data presented in their work are very useful as benchmarks for future characterization of Li₂O₂ during the discharge of Li-air cells. Also note that NIXS using hard X-rays is a suitable analytical technique for providing bulk sensitive information on Li-air battery discharge products with element specificity [23]. Also known as X-ray Raman scattering, NIXS can be considered as an alternative approach toward obtaining soft X-ray absorption spectroscopy (XAS)-like information using hard X-rays, despite crystalline or amorphous components being present.

Figure 12. (a) Féher's; (b) density functional theory (DFT)-relaxed Féher's according to Cota; and (c) Föppl's proposed crystal structures for Li₂O₂. Red (larger) spheres represent oxygen atoms and blue (smaller) spheres represent lithium atoms. Blue (dashed) horizontal lines indicate Li planes. We can see that Li atoms are roughly in-plane with the O atoms in the Féher structure while Li planes cut through the O–O bonds in the Föppl structure. Reprinted with permission [28]; Copyright 2011, American Chemical Society.



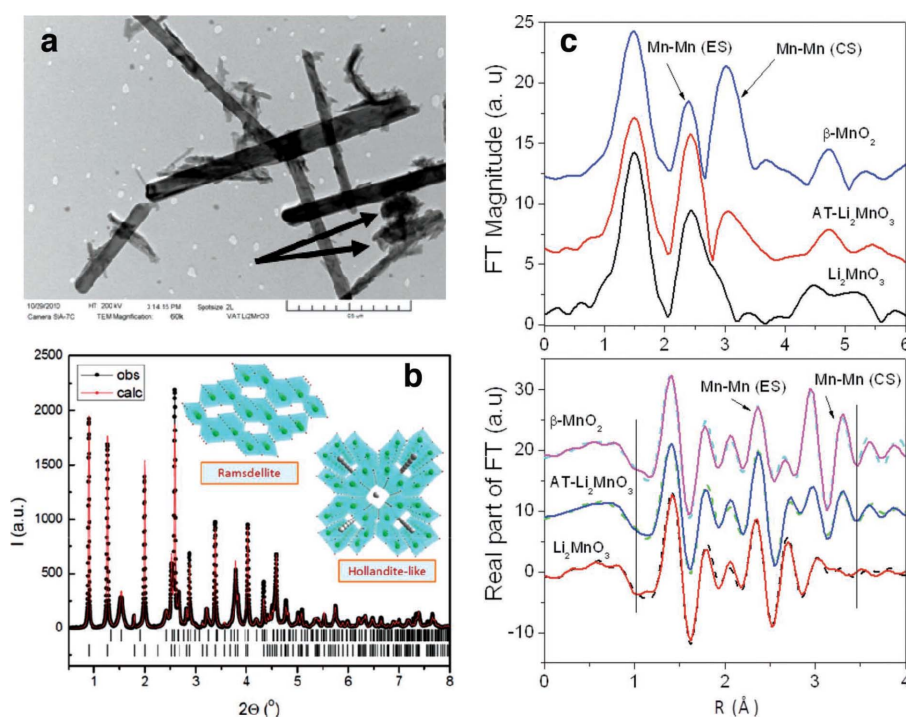
Using DFT together with classical statistical mechanical analyses, Lau and Curtiss [25] investigated the thermodynamic stability of bulk crystalline LiO_2 , Li_2O , and Li_2O_2 as a function of the oxygen environment, which is relevant to the basic bulk Li-O_2 electrochemical couples observed in the Li-air battery. Their calculated results demonstrated that $\text{Li}_2\text{O}_2(\text{s})$ and superoxide [$\text{LiO}_2(\text{s})$] are likely to be stable only under O_2 -rich conditions with high oxygen partial pressures, whereas Li_2O is most stable at ambient conditions.

5. Air-Breathing Cathode

Cathode materials represent a major technology challenge in rechargeable Li-air battery development. The specific capacity and power capability of Li-air cells strongly depend on the materials and microstructures of the air-breathing cathode, which contribute to most of its voltage drop [3,6,76,77]. A high performance cathode should be able to provide: (a) good electronic and ionic conductivity; (b) fast oxygen diffusion; and (c) stable electrode integrity. It should also have an efficient catalyst supported by a high surface area substrate, similar to that in a proton exchange membrane fuel cell. Since the first demonstration of a lithium-oxygen system using pyrolyzed cobalt phthalocyanine over carbon as the cathode [63], many new cathode materials have been reported, particularly in the area of new catalysts for improving the battery efficiency [8,40,42,44,62].

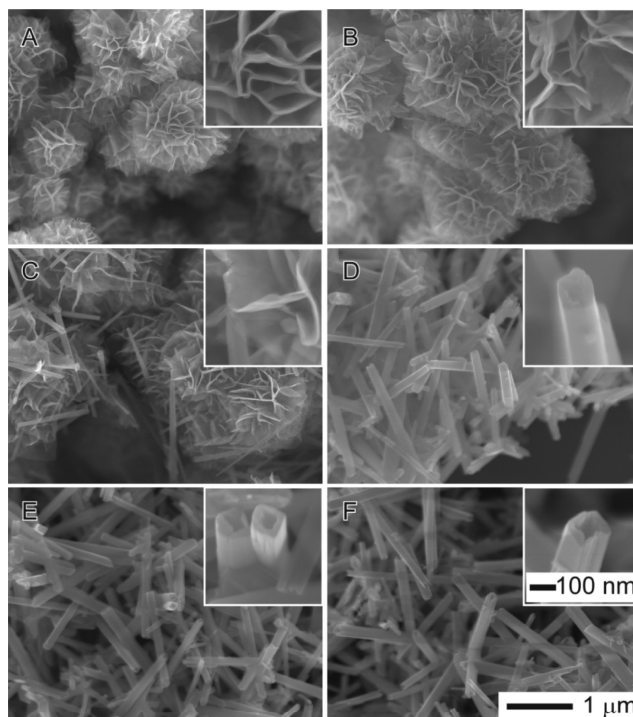
In 2006, Bruce *et al.* [2] demonstrated high-energy-density Li-air cells using a porous carbon cathode with electrolytic manganese dioxide. Since that time, MnO_2 -based compounds have been widely investigated as the cathode catalyst to improve the performance of the air-breathing cathode. In their study, they found that different catalytic reactivity for the oxygen evolution reaction could be achieved for MnO_2 with different crystal structures and morphologies, among which the use of α - MnO_2 nanowires was found to deliver capacities of 3000 mA h/g of carbon [78]. Several manganese dioxide materials have been investigated as electrocatalysts for non-aqueous Li-air cells, which were prepared by various approaches with different crystalline structures and morphologies [9,10,17]. One is MnO_2 with a “tunnel” structure reported by Trahey *et al.* [10], meaning there are parallel, one-dimensional lines of open space through the structures. In their work, they produced nanostructured MnO_2 with dual electrode/electrocatalyst functionality that has an affinity to react with Li_2O by treating Li_2MnO_3 ($\text{Li}_2\text{O}\cdot\text{MnO}_2$) with highly concentrated acid. Both XRD and XAS measurements showed that the acid-treated Li_2MnO_3 electrodes consist of a composite α - MnO_2 /ramsdellite- MnO_2 product with a one-to-one ratio between corner-shared and edge-shared oxygen octahedral around Mn ions. This finding confirms the presence of tunnels in the parent structure, as shown in Figure 13. Transmission electron microscopy (TEM) (Figure 13a) revealed the existence of nanorod-shaped particles. The presence of such MnO_2 catalyst on the cathode reduces the charging potential of the cell. As determined by XPS, the discharge products (solids) formed using PC as the electrolyte appeared to be lithium carbonate and lithium oxide, and lithium oxide disappeared upon charge. These results suggest that the α - MnO_2 /ramsdellite- MnO_2 catalyst is playing a key role in the reversibility of the lithium oxide products, even though evidence suggests that PC is partially decomposing during the discharge/charge cycles.

Figure 13. (a) Transmission electron microscopy (TEM) image of α -MnO₂ needles and R-MnO₂ crystallites (arrowed); (b) observed and calculated X-ray powder diffraction of the acid-treated Li₂MnO₃ product, with schematic structures of the α -MnO₂ and ramsdellite-MnO₂ components; the short vertical lines indicate the peak positions of the two phases; (c, top) phase uncorrected Fourier transform (FT) magnitude of Mn K-edge extended X-ray absorption fine structure (EXAFS) (k^3 weighted) for acid-treated Li₂MnO₃ and Li₂MnO₃ and β -MnO₂ standards. The peaks at ~ 2.4 Å and ~ 3.1 Å arise due to edge sharing (ES) and corner sharing (CS) Mn–Mn correlations from MnO₆ octahedral linkages, respectively; and (c, bottom) R-space fits (solid line) of the real part of the FT of Mn EXAFS data along with the experimental data (dashed lines). The vertical lines show the fit range covered. Reprinted with permission [10]; Copyright 2013, Wiley-VCH Verlag GmbH & Co. KGaA, Weinheim.



Since MnO₂ nanoparticles can exhibit various crystallographic structures (e.g., α , β , δ , γ , and λ forms) and morphologies, controlled synthesis of nanostructured MnO₂ with high crystalline purity and uniform morphology is critical to precisely tailored properties and better performance in Li-air batteries. To address this issue, Truong *et al.* [9] produced high-quality nanosheet-based δ -MnO₂ microflowers, α -MnO₂ nanowires, and α -MnO₂ nanotubes in large quantity through microwave-assisted hydrothermal reduction of potassium permanganate in the presence of hydrochloric acid, as shown in Figure 14. They found that the chemical reaction determines the formation of δ -MnO₂ microflowers in the earlier stage of the process, while the two-step Ostwald ripening process dominates the crystalline and morphological transition from the δ -MnO₂ nanosheets to α -MnO₂ nanowires and nanotubes in the late stage of the reactions. In terms of the electrocatalytic activity for these MnO₂ nanoparticles, the single-crystal α -MnO₂ nanotubes exhibit much better performance to catalyze the electrochemical processes involved in Li-air batteries, leading to a significant improvement in specific capacity and cycle life.

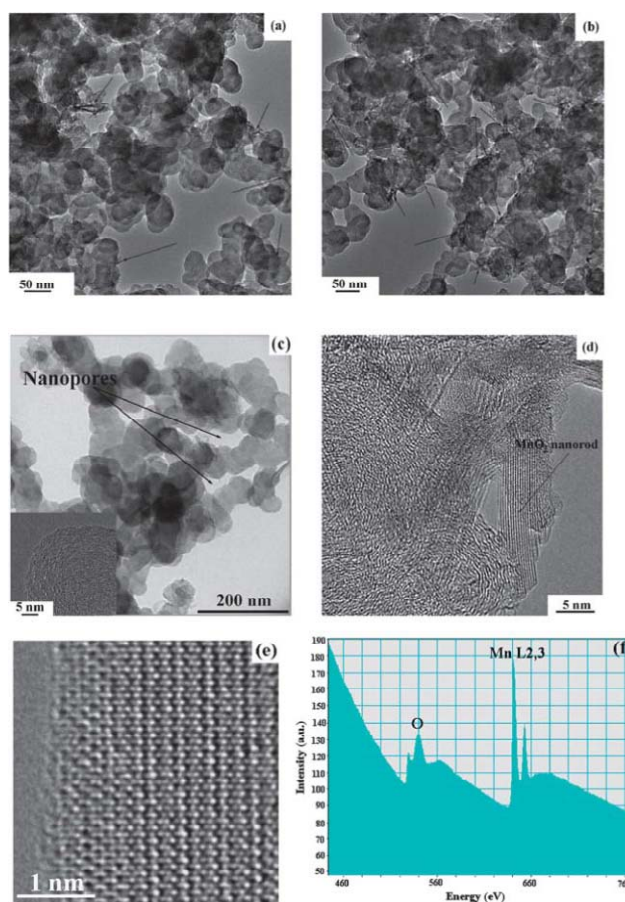
Figure 14. SEM images of MnO₂ products obtained at different reaction times: (A) 2; (B) 5; (C) 15; (D) 30; (E) 120; and (F) 360 min. The temperature of the reaction solutions and the atmosphere pressure above the reaction solutions were 150 °C and 70 psi, respectively. The concentrations of KMnO₄ and HCl in the reaction solution were 0.05 and 0.2 M, respectively, before the reaction was initiated. The insets are the high-magnification SEM images of the corresponding structures. The scale bars in (F) also apply to (A)–(E). Reprinted with permission [9]; Copyright 2013, American Chemical Society.



The high surface area and porous structure of the carbon cathode are critical for the high electrochemical performance of Li-air batteries. In general, a larger surface area provides more surface to uniformly disperse catalytic particles and more active sites to aid the electrochemical reactions, while a porous structure with an appropriate pore size provides the space to store the discharge products. However, a problem has been encountered in previous studies [2,16,55,78], because the catalysts are pre-synthesized and then loaded onto carbon support by blending with carbon powder. This process introduces not only the potential of destroying the porous structure of the carbon support, if high-energy ball milling is applied, but also the non-uniform dispersion of the catalysts on the carbon support. Aiming to develop a new method to uniformly disperse the catalyst onto the carbon support while still preserving the original porous structure of carbon during the synthesis, Qin *et al.* [17] developed an *in-situ* wet-chemistry approach to incorporate MnO₂ nanoparticles into porous carbon, which avoids any aggressive post-treatment of the carbon materials and thus preserves the original structure of the carbon matrix. The TEM images in Figure 15 clearly indicate that most of the as-prepared MnO₂ particles are uniformly dispersed onto the carbon matrix with rod-like shape. The SEM images of the samples before and after being loaded with MnO₂ catalysts confirm that the porous structure of carbon was well preserved during the synthesis process. These as-prepared MnO₂/C composites with porous structures and high specific surface area provide more active sites for enabling the oxygen

reduction and oxygen evolution reactions, and, therefore, lead to significant enhancement of cell performance. The as-prepared MnO₂/C composite cathode achieved a low charge overpotential (3.5 V) in a cell tested with a TEGDME-based electrolyte.

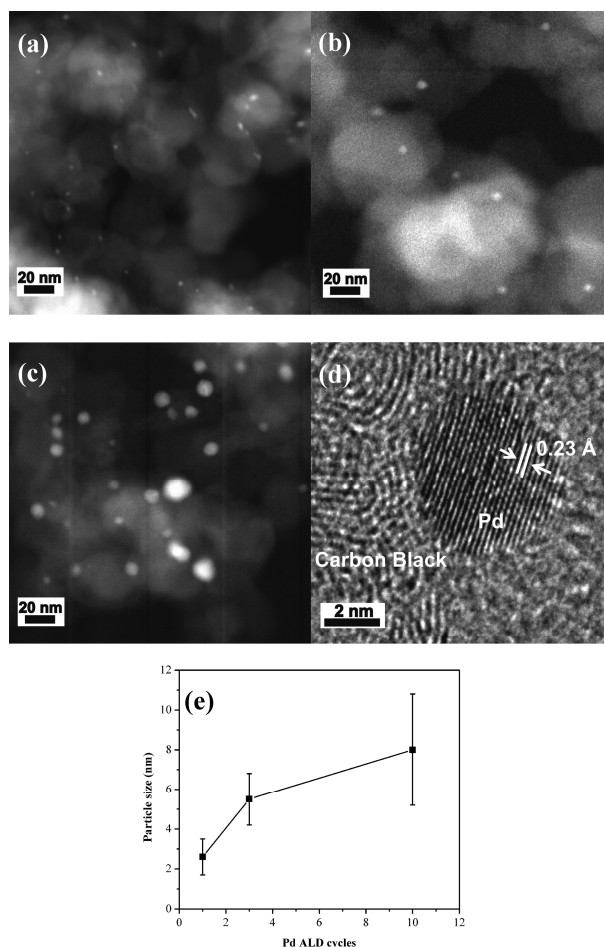
Figure 15. TEM images of (a) as-prepared MnO₂/C composite (Sample 1); (b) as-prepared MnO₂/C composite (Sample 2); and (c) original Super P Li (SPL) carbon; (d) and (e) high-resolution transmission electron microscopy (HRTEM) image of Sample 1; and (f) electron energy loss spectra (EELS) of Sample 1. Reproduced from [17] with permission from The Royal Society of Chemistry.



Recently, Lei *et al.* [30] also employed atomic layer deposition (ALD) for dispersing Pd catalysts with well-controlled particle size uniformly onto the carbon support. The ALD technique is capable of depositing highly uniform and conformal coatings on surfaces with complex topographies and infiltrating mesoporous materials [79–81]. This capability is particularly attractive for the synthesis of heterogeneous catalysts requiring highly dispersed catalytic species on high-surface-area mesoporous supports. The good dispersion of the active particles on the support during ALD decreases the metal loading while still achieving the same catalytic activity as the catalysts with higher metal loading prepared by other methods. This feature is especially important with noble metal materials, where the excess use of the raw materials should be avoided. Lei *et al.* [30] demonstrated that the Pd nanoparticles can be uniformly distributed on the porous carbon surface with average particle size controlled by the number of ALD Pd cycles to be in the range of 2–8 nm, as shown in scanning transmission electron microscopy (STEM) images (Figure 16). Such Pd/C composites with porous

structures and high specific surface area provide more active sites to absorb O_2 molecules and, therefore, enhance the catalytic activity for the oxygen reduction reaction, as evident by a significantly higher discharge capacity achieved in the Li-air cell.

Figure 16. Scanning transmission electron microscopy (STEM) images of (a) 1c Pd/C; (b) 3c Pd/C; (c) 10c Pd/C; (d) HRTEM of a Pd nanoparticle ~ 5.5 nm in diameter prepared by atomic layer deposition (ALD) supported over carbon; (e) Pd particle size as a function of ALD cycles. Reprinted with permission [30]; Copyright 2013, American Chemical Society.



In addition, several Fe-based electrocatalysts were successfully incorporated to carbon supports and tested in the Li-air cells as the active cathode materials. For instance, Trahey *et al.* [16] designed electrocatalysts by either electrochemical activation of Li_5FeO_4 ($5Li_2O \cdot Fe_2O_3$) or acid activation of $Li_2MnO_3 \cdot LiFeO_2$ ($[Li_2O \cdot MnO_2] \cdot [Li_2O \cdot Fe_2O_3]$) to remove Li_2O , which delivers high discharge capacity. Lu *et al.* [34] synthesized a uniformly dispersed core-shelled Fe/ Fe_3O_4 nanocomposite on porous carbon via a wet-chemistry approach, which was tested as a cathode material in the Li-air battery, showing an enhanced catalytic effect toward the electrochemical reactions, in particular, the oxygen reduction reaction. The XRD and XPS data demonstrated that Li_2O_2 participated in the reversible reactions in a Li- O_2 cell with TEGDME-based electrolyte. Shui *et al.* [19] produced a Fe/N/C composite via pyrolysis of an organometallic precursor at high temperature and evaluated its catalytic performance in connection with the rechargeable Li-air battery. Compared with the well-studied α - MnO_2 /XC-72 composite and its unmodified carbon-only counterpart, this chemically modified

carbon exhibited lower charge-discharge overpotential and improved the battery lifespan. A gas analysis at the end of discharge-charge cycling found no CO₂ formation for the cathode made with Fe/N/C catalyst, despite the charge potential exceeding 4.0 V. According to the authors, the catalytic selectivity of the Fe/N/C composite promotes the decomposition of Li₂O₂ over that of the electrolyte and, therefore, leads to an enhanced battery lifespan under controlled cycling.

6. Oxygen Crossover Effect on Lithium Anode

As discussed above, the current major focus of studies on Li-air batteries has been the roles that electrolyte decomposition and the catalytic air cathode play in the cell performance. It is well established that the electrolyte decomposition mainly arises from chemical or electrochemical reactions at the electrolyte-cathode interface and electrolyte-Li₂O₂ interface. However, another source of detrimental electrolyte decomposition in Li-air batteries, which has not been investigated in much detail yet, could be electrolyte decomposition at the lithium anode. In Li-ion batteries, reactions at the Li anode are a problem (dendrite formation), which is much more severe for Li-O₂ batteries considering the presence of the oxygen environment. Because the separators currently used in Li-air cells cannot prevent O₂ diffusion to the anode, oxygen crossover can be a significant problem, leading to fast decay of the Li anode.

Recently, Assary *et al.* [12] performed experimental and computational studies focused on the possible reactions that may occur at the lithium anode under conditions used in a TEGDME-based Li-O₂ cell, where oxygen crossover occurs. DFT calculation indicated that the presence of O₂ from an oxygen crossover effect from the cathode to the anode results in favorable subsequent reaction pathways, since the binding of O₂ with the TEGDME anion radical is exothermic by 3.3 eV. Due to the larger electron affinity of TEGDME, the electron is transferred to O₂ upon binding of O₂ to the reduced species. The subsequent cleavage of the C–O bond of the ether by these O₂ anion radicals is no apparent barrier due to the large exothermicity of the first step (A → B), as shown in Figure 17. This reaction pathway can lead to the formation of various alkoxy radicals, the hydroxide ion, and aldehydes. The hydroxide ion can then bind to a Li cation in solution to form LiOH and, as the concentration of this species increases, it will result in the formation of insoluble LiOH on the anode. Further reduction and reaction with O₂ of the other fragments (alkoxy radicals and aldehydes) can lead to the formation of lithium alkylcarbonates or lithium carbonates, which may end up on the Li anode as well. In order to investigate potential products that are formed at the anode in a Li-air battery, they have carried out a detailed characterization study of the anode during various stages of discharge and charge using *in-situ* XRD measurements. The *in-situ* XRD data shown in Figure 18 clearly indicate the formation of LiOH and Li₂CO₃ on cycling, which confirm the theoretical prediction as discussed above. This study provides evidence that controlling reactions of electrolytes at the lithium anode through suitable membranes or passivation films is essential for achieving good performance of Li-air cells.

Figure 17. Proposed mechanism and energetics for the formation of LiOH from an ether-based solvent (TEGDME) at the anode upon reduction and oxygen crossover. Also shown in the box is a mechanism for the further formation of lithium alkyl carbonates and carbonates from resulting aldehydes. All energetics are changes in enthalpies (eV) in solution ($\epsilon = 21$) at 298 K computed at the B3LYP/6-31+G(d) level of theory (see supporting information for details of computation in [12]). Reprinted with permission [12]; Copyright 2013, Wiley-VCH Verlag GmbH & Co. KGaA, Weinheim.

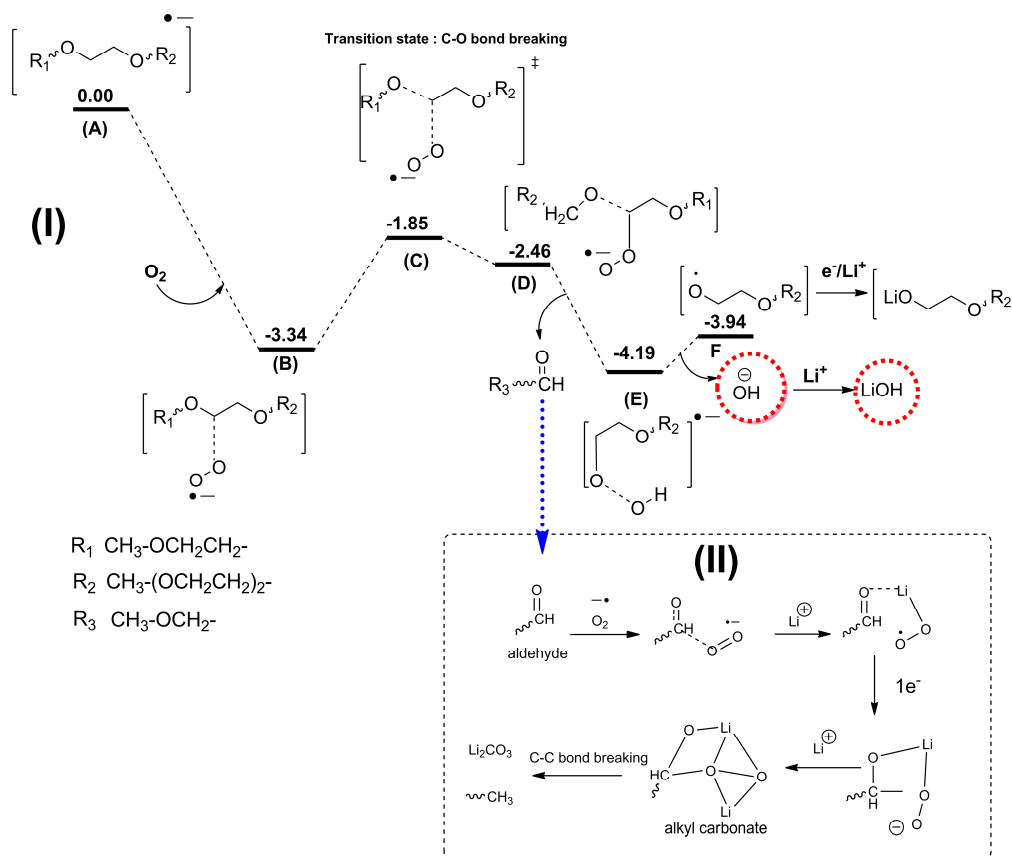
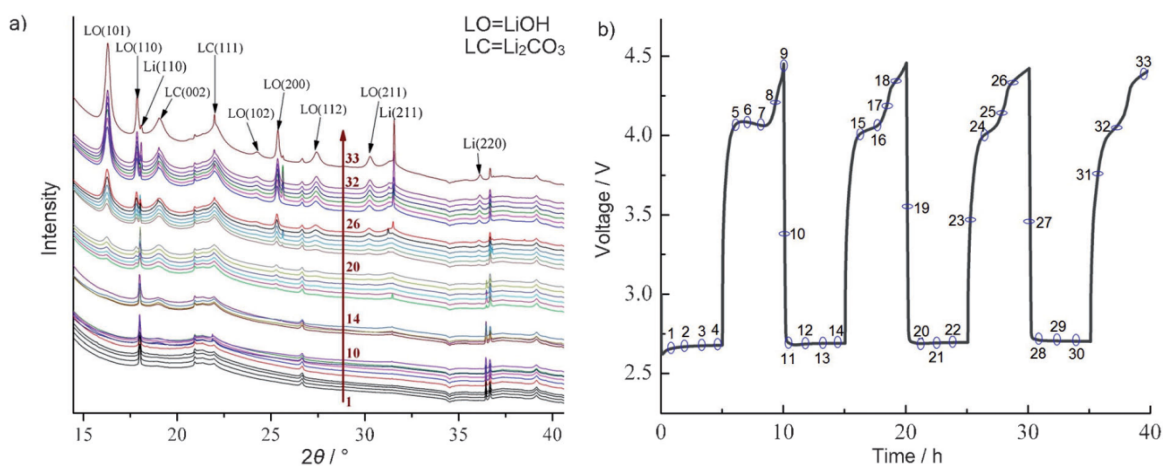
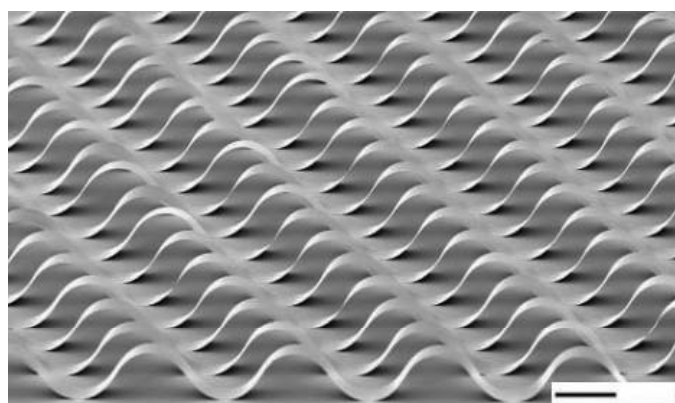


Figure 18. (a) *In situ* XRD patterns of Li anode and LiOH formation during the operations conditions; and (b) corresponding voltage vs. time profile. Numbers on XRD data correspond to those on voltage profile. Reprinted with permission [12]; Copyright 2013, Wiley-VCH Verlag GmbH & Co. KGaA, Weinheim.



To eliminate the O₂ crossover to the anode responsible for limiting the reversibility of Li-air cells, it is critical to develop thin, active membranes that can be embedded within passive porous polymeric membranes, which serve as the supports. These composite membranes should meet the following criteria for successful implementation in a rechargeable Li-air cell: (1) block diffusion of oxygen from the air cathode to the lithium anode; (2) allow the transport of lithium ions to support current flow; and (3) exhibit excellent mechanical flexibility and stability to be compatible with the mechanical flexibility of the supporting polymer membranes and battery design/processing. Engineering the active membranes with a nanometer-scale thickness could potentially meet these criteria. As an example, nanoribbons of single-crystal silicon with thickness of 100 nm exhibit buckled geometries and mechanical flexibilities on a rubber substrate, as shown in Figure 19 [82].

Figure 19. Structure nanoribbons of single crystal silicon with a thickness of 100 nm (scale bar 100 μm). Reprinted with permission [82]; Copyright 2006, Nature Publishing Group.



Truong *et al.* [11] fabricated single-crystal silicon membranes with high lithium conductivity and tested them in Li-air batteries. Their results demonstrated that the single-crystal Si membranes are capable of conducting Li⁺ ions through their lattices to support current density as high as 1 mA/cm². However, compared with the best NASICON-type lithium ion conducting membranes (LICMs), the Li⁺ conductivity of the single-crystal Si membranes is still too low (3–4 orders lower). Their ionic conductivity might be improved by doping the surface lattices of single-crystal Si membranes, lowering the interfacial energy barriers for Li⁺ insertion/extraction from the Si lattices, or partially lithiating the single-crystal Si membranes to increase the concentration of Li⁺ ions in the membranes and thereby reduce their diffusive resistance. Direct contact of the single-crystal Si membranes with Li metal should be avoided due to the severe electrochemical reactions, although the Si membranes are stable in many electrolytes, including neutral/acidic aqueous electrolytes and aprotic organic electrolytes. More detail about Li-ion conducting membranes for the Li-air battery application can be found in a recent review article by Sun [29].

7. Concluding Remarks

Rechargeable non-aqueous Li-air battery technology is still at the infant stage, although significant progress has been made, as summarized in this article. We have reviewed the research activities on non-aqueous Li-air batteries at Argonne National Laboratory, which cover the stability of the

electrolyte and its influence on the electrochemical performance, structure and magnetic properties of Li_2O_2 and their relevance to Li-air battery design, the design and optimization of the air cathode structure with different types of catalyst, the oxygen crossover effect on the Li anode as determined by both experimental and theoretical modeling results, and the development of a single-crystal silicon membrane with high lithium conductivity.

The main challenges at the current stage for Li-air batteries are the instability of the aprotic electrolyte and the low round-trip efficiency (high charge overpotential). Carbonate-based electrolytes have been widely used in most initial research, but it is now universally recognized that these electrolytes decompose in the presence of the superoxide radicals. Ether-based electrolytes seem to be relatively stable against the discharge products, but their stability during charge, especially at high voltage, remains unclear. Searching for new electrolytes that are fully stable on cycling will be critical to developing Li-air batteries, although it will be very challenging. In parallel with the importance of the electrolytes, investigation on how the porous air cathode architectures affect the formation of the discharge product, Li_2O_2 , and overall capacity of the cell is still greatly needed. In terms of protecting the Li anode from the oxygen crossover, controlling reactions of electrolytes at the anode through suitable membranes or passivation films will be essential for achieving good performance. Study of the cell during discharge and charge using in-situ high-energy X-ray techniques is expected to provide insight into the structural changes at the atomic level, as presented in this review. X-ray absorption fine structure spectroscopy (XAFS) is another powerful tool for studies of the electronic and atomic structure of the catalysts in action, which allows in-situ characterization in a suitably designed cell or reactor.

Acknowledgments

This work was supported by the U.S. Department of Energy under Contract DE-AC0206CH11357 with the main support provided by the Vehicle Technologies Office, Department of Energy (DOE) Office of Energy Efficiency and Renewable Energy (EERE). J. Lu was supported by the DOE Office of EERE Postdoctoral Research Award under the EERE Vehicles Technology Program administered by the Oak Ridge Institute for Science and Education (ORISE) for the DOE.

Conflicts of Interest

The authors declare no conflict of interest.

References

1. Yang, Z.; Zhang, J.; Kintner-Meyer, M.C.W.; Lu, X.; Choi, D.; Lemmon, J.P.; Liu, J. Electrochemical energy storage for green grid. *Chem. Rev.* **2011**, *111*, 3577–3613.
2. Ogasawara, T.; Debart, A.; Holzapfel, M.; Novak, P.; Bruce, P.G. Rechargeable Li_2O_2 electrode for lithium batteries. *J. Am. Chem. Soc.* **2006**, *128*, 1390–1393.
3. Beattie, S.D.; Manolescu, D.M.; Blair, S.L. High-capacity lithium-air cathodes. *J. Electrochem. Soc.* **2009**, *156*, A44–A47.

4. Wang, Y.; Zhou, H. A lithium-air fuel cell using copper to catalyze oxygen-reduction based on copper-corrosion mechanism. *Chem. Commun.* **2010**, *46*, 6305–6307.
5. Bruce, P.G.; Hardwick, L.J.; Abraham, K.M. Lithium-air and lithium-sulfur batteries. *MRS Bull.* **2011**, *36*, 506–512.
6. Xiao, J.; Mei, D.; Li, X.; Xu, W.; Wang, D.; Graff, G.L.; Bennett, W.D.; Nie, Z.; Saraf, L.V.; Aksay, I.A.; *et al.* Hierarchically porous graphene as a lithium-air battery electrode. *Nano Lett.* **2011**, *11*, 5071–5078.
7. Chen, Y.; Freunberger, S.A.; Peng, Z.; Fontaine, O.; Bruce, P.G. Charging a Li-O₂ battery using a redox mediator. *Nat. Chem.* **2013**, *5*, 489–494.
8. Cheng, F.; Liang, J.; Tao, Z.; Chen, J. Functional materials for rechargeable batteries. *Adv. Mater.* **2011**, *23*, 1695–1715.
9. Truong, T.T.; Liu, Y.; Ren, Y.; Trahey, L.; Sun, Y. Morphological and crystalline evolution of nanostructured MnO₂ and its application in lithium-air batteries. *ACS Nano* **2012**, *6*, 8067–8077.
10. Trahey, L.; Karan, N.K.; Chan, M.K.Y.; Lu, J.; Ren, Y.; Greeley, J.; Balasubramanian, M.; Burrell, A.K.; Curtiss, L.A.; Thackeray, M.M. Synthesis, characterization, and structural modeling of high-capacity, dual functioning MnO₂ electrode/electrocatalysts for Li-O₂ cells. *Adv. Energy Mater.* **2013**, *3*, 75–84.
11. Truong, T.T.; Qin, Y.; Ren, Y.; Chen, Z.; Chan, M.K.; Greeley, J.P.; Amine, K.; Sun, Y. Single-crystal silicon membranes with high lithium conductivity and application in lithium-air batteries. *Adv. Mater.* **2011**, *23*, 4947–4952.
12. Assary, R.S.; Lu, J.; Du, P.; Luo, X.; Zhang, X.; Ren, Y.; Curtiss, L.A.; Amine, K. The effect of oxygen crossover on the anode of a Li-O₂ battery using an ether-based solvent: Insights from experimental and computational studies. *ChemSusChem* **2013**, *6*, 51–55.
13. Lu, J.; Jung, H.-J.; Lau, K.C.; Zhang, Z.; Schlueter, J.A.; Du, P.; Assary, R.S.; Greeley, J.; Ferguson, G.A.; Wang, H.-H.; *et al.* Magnetism in lithium-oxygen discharge product. *ChemSusChem* **2013**, *6*, 1196–1202.
14. Shui, J.-L.; Okasinski, J.S.; Zhao, D.; Almer, J.D.; Liu, D.-J. Microfocused X-ray study on precipitate formation in the separator region of nonaqueous Li-O₂ batteries. *ChemSusChem* **2012**, *5*, 2421–2426.
15. Shui, J.-L.; Wang, H.-H.; Liu, D.-J. Degradation and revival of Li-O₂ battery cathode. *Electrochem. Commun.* **2013**, *34*, 45–47.
16. Trahey, L.; Johnson, C.S.; Vaughey, J.T.; Kang, S.H.; Hardwick, L.J.; Freunberger, S.A.; Bruce, P.G.; Thackeray, M.M. Activated lithium-metal-oxides as catalytic electrodes for Li-O₂ cells. *Electrochem. Solid-State Lett.* **2011**, *14*, A64–A66.
17. Qin, Y.; Lu, J.; Du, P.; Chen, Z.; Ren, Y.; Wu, T.; Miller, J.T.; Wen, J.; Miller, D.J.; Zhang, Z.; *et al.* *In situ* fabrication of porous-carbon-supported α -MnO₂ nanorods at room temperature: Application for rechargeable Li-O₂ batteries. *Energy Environ. Sci.* **2013**, *6*, 519–531.
18. Shui, J.; Okasinski, J.; Zhao, D.; Almer, J.; Liu, D.-J. Understanding of electrolyte stability and its impact of lifespan of Li-O₂ battery. *ESC Trans.* **2013**, *50*, 37–45.
19. Shui, J.-L.; Karan, N.K.; Balasubramanian, M.; Li, S.-Y.; Liu, D.-J. Fe/N/C composite in Li-O₂ battery: Studies of catalytic structure and activity toward oxygen evolution reaction. *J. Am. Chem. Soc.* **2012**, *134*, 16654–16661.

20. Ryan, K.R.; Trahey, L.; Okasinski, J.S.; Burrell, A.K.; Ingram, B.J. *In situ* synchrotron X-ray diffraction studies of lithium oxygen batteries. *J. Mater. Chem. A* **2013**, *1*, 6915–6919.
21. Assary, R.S.; Curtiss, L.A.; Redfern, P.C.; Zhang, Z.; Amine, K. Computational studies of polysiloxanes: Oxidation potentials and decomposition reactions. *J. Phys. Chem. C* **2011**, *115*, 12216–12223.
22. Assary, R.S.; Lau, K.C.; Amine, K.; Sun, Y.-K.; Curtiss, L.A. Interactions of dimethoxy ethane with Li₂O₂ clusters and likely decomposition mechanisms for Li-O₂ batteries. *J. Phys. Chem. C* **2013**, *117*, 8041–8049.
23. Karan, N.K.; Balasubramanian, M.; Fister, T.T.; Burrell, A.K.; Du, P. Bulk-sensitive characterization of the discharged products in Li-O₂ batteries by nonresonant inelastic X-ray scattering. *J. Phys. Chem. C* **2012**, *116*, 18132–18138.
24. Lau, K.C.; Assary, R.S.; Redfern, P.; Greeley, J.; Curtiss, L.A. Electronic structure of lithium peroxide clusters and relevance to lithium-air batteries. *J. Phys. Chem. C* **2012**, *116*, 23890–23896.
25. Lau, K.C.; Curtiss, L.A.; Greeley, J. Density functional investigation of the thermodynamic stability of lithium oxide bulk crystalline structures as a function of oxygen pressure. *J. Phys. Chem. C* **2011**, *115*, 23625–23633.
26. Ryan, K.R.; Trahey, L.; Ingram, B.J.; Burrell, A.K. Limited stability of ether-based solvents in lithium-oxygen batteries. *J. Phys. Chem. C* **2012**, *116*, 19724–19728.
27. Zhang, Z.C.; Lu, J.; Assary, R.S.; Du, P.; Wang, H.H.; Sun, Y.K.; Qin, Y.; Lau, K.C.; Greeley, J.; Redfern, P.C.; *et al.* Increased stability toward oxygen reduction products for lithium-air batteries with oligoether-functionalized silane electrolytes. *J. Phys. Chem. C* **2011**, *115*, 25535–25542.
28. Chan, M.K.Y.; Shirley, E.L.; Karan, N.K.; Balasubramanian, M.; Ren, Y.; Greeley, J.P.; Fister, T.T. Structure of lithium peroxide. *J. Phys. Chem. Lett.* **2011**, *2*, 2483–2486.
29. Sun, Y. Lithium ion conducting membranes for lithium-air batteries. *Nano Energy* **2013**, *2*, 801–816.
30. Lei, Y.; Lu, J.; Luo, X.; Wu, T.; Du, P.; Zhang, X.; Ren, Y.; Wen, J.; Miller, D.J.; Miller, J.T.; *et al.* Synthesis of porous carbon supported palladium nanoparticle catalysts by atomic layer deposition: Application for rechargeable lithium-O₂ battery. *Nano Lett.* **2013**, *13*, 4182–4189.
31. Shui, J.-L.; Okasinski, J.S.; Kenesei, P.; Dobbs, H.A.; Zhao, D.; Almer, J.D.; Liu, D.-J. Reversibility of anodic lithium in rechargeable lithium-oxygen batteries. *Nat. Commun.* **2013**, *4*, doi:10.1038/ncomms3255.
32. Du, P.; Lu, J.; Lau, K.C.; Luo, X.; Bareno, J.; Zhang, X.; Ren, Y.; Zhang, Z.; Curtiss, L.A.; Sun, Y.-K.; *et al.* Compatibility of lithium salts with solvent of the non-aqueous electrolyte in Li-O₂ batteries. *Phys. Chem. Chem. Phys.* **2013**, *15*, 5572–5578.
33. Yang, J.; Zhai, D.; Wang, H.-H.; Lau, K.C.; Schlueter, J.A.; Du, P.; Myers, D.J.; Sun, Y.-K.; Curtiss, L.A.; Amine, K. Evidence for lithium superoxide-like species in the discharge product of a Li-O₂ battery. *Phys. Chem. Chem. Phys.* **2013**, *15*, 3764–3771.
34. Lu, J.; Qin, Y.; Du, P.; Luo, X.; Wu, T.; Ren, Y.; Wen, J.; Miller, D.J.; Miller, J.T.; Amine, K. Synthesis and characterization of uniformly dispersed Fe₃O₄/Fe nanocomposite on porous carbon: Application for rechargeable Li-O₂ batteries. *RSC Adv.* **2013**, *3*, 8276–8285.
35. Shao, Y.; Park, S.; Xiao, J.; Zhang, J.-G.; Wang, Y.; Liu, J. Electrocatalysts for nonaqueous lithium-air batteries: Status, challenges, and perspective. *ACS Catal.* **2012**, *2*, 844–857.

36. Black, R.; Adams, B.; Nazar, L.F. Non-aqueous and hybrid Li-O₂ batteries. *Adv. Energy Mater.* **2012**, *2*, 801–815.
37. Cao, R.; Lee, J.-S.; Liu, M.; Cho, J. Recent progress in non-precious catalysts for metal-air batteries. *Adv. Energy Mater.* **2012**, *2*, 816–829.
38. Lee, J.-S.; Kim, S.T.; Cao, R.; Choi, N.-S.; Liu, M.; Lee, K.T.; Cho, J. Metal-air batteries with high energy density: Li-air versus Zn-air. *Adv. Energy Mater.* **2011**, *1*, 34–50.
39. Park, M.; Sun, H.; Lee, H.; Lee, J.; Cho, J. Lithium-air batteries: Survey on the current status and perspectives towards automotive applications from a battery industry standpoint. *Adv. Energy Mater.* **2012**, *2*, 780–800.
40. Shao, Y.; Ding, F.; Xiao, J.; Zhang, J.; Xu, W.; Park, S.; Zhang, J.-G.; Wang, Y.; Liu, J. Making Li-air batteries rechargeable: Material challenges. *Adv. Funct. Mater.* **2013**, *23*, 987–1004.
41. Ellis, B.L.; Lee, K.T.; Nazar, L.F. Positive electrode materials for Li-ion and Li-batteries. *Chem. Mater.* **2010**, *22*, 691–714.
42. Cheng, F.; Chen, J. Metal-air batteries: From oxygen reduction electrochemistry to cathode catalysts. *Chem. Soc. Rev.* **2012**, *41*, 2172–2192.
43. Jeong, G.; Kim, Y.-U.; Kim, H.; Kim, Y.-J.; Sohn, H.-J. Prospective materials and applications for Li secondary batteries. *Energy Environ. Sci.* **2011**, *4*, 1986–2002.
44. Li, F.; Zhang, T.; Zhou, H. Challenges of non-aqueous Li-O₂ batteries: Electrolytes, catalysts, and anodes. *Energy Environ. Sci.* **2013**, *6*, 1125–1141.
45. Christensen, J.; Albertus, P.; Sanchez-Carrera, R.S.; Lohmann, T.; Kozinsky, B.; Liedtke, R.; Ahmed, J.; Kojic, A. A critical review of Li/air batteries. *J. Electrochem. Soc.* **2012**, *159*, R1–R30.
46. Girishkumar, G.; McCloskey, B.; Luntz, A.C.; Swanson, S.; Wilcke, W. Lithium-air battery: Promise and challenges. *J. Phys. Chem. Lett.* **2010**, *1*, 2193–2203.
47. Capsoni, D.; Bini, M.; Ferrari, S.; Quartarone, E.; Mustarelli, P. Recent advances in the development of Li-air batteries. *J. Power Sources* **2012**, *220*, 253–263.
48. Kraetsberg, A.; Yair, E.-E. Review on Li-air batteries-opportunities, limitations and perspective. *J. Power Sources* **2011**, *196*, 886–893.
49. Padbury, R.; Zhang, X. Lithium-oxygen batteries-limiting factors that affect performance. *J. Power Sources* **2011**, *196*, 4436–4444.
50. Song, M.-K.; Park, S.; Alamgir, F.M.; Cho, J.; Liu, M. Nanostructured electrodes for lithium-ion and lithium-air batteries: The latest developments, challenges, and perspectives. *Mater. Sci. Eng. R Rep.* **2011**, *72*, 203–252.
51. Bruce, P.G.; Freunberger, S.A.; Hardwick, L.J.; Tarascon, J.-M. Li-O₂ and Li-S batteries with high energy storage. *Nat. Mater.* **2012**, *11*, 19–29.
52. Black, R.; Oh, S.H.; Lee, J.-H.; Yim, T.; Adams, B.; Nazar, L.F. Screening for superoxide reactivity in Li-O₂ batteries: Effect on Li₂O₂/LiOH crystallization. *J. Am. Chem. Soc.* **2012**, *134*, 2902–2905.
53. Lim, H.-K.; Lim, H.-D.; Park, K.-Y.; Seo, D.-H.; Gwon, H.; Hong, J.; Goddard, W.A.; Kim, H.; Kang, K. Toward a lithium-“air” battery: The effect of CO₂ on the chemistry of a lithium-oxygen cell. *J. Am. Chem. Soc.* **2013**, *135*, 9733–9742.
54. Lu, Y.-C.; Gasteiger, H.A.; Shao-Horn, Y. Catalytic activity trends of oxygen reduction reaction for nonaqueous Li-air batteries. *J. Am. Chem. Soc.* **2011**, *133*, 19048–19051.

55. Lu, Y.-C.; Xu, Z.; Gasteiger, H.A.; Chen, S.; Hamad-Schifferli, K.; Shao-Horn, Y. Platinum-gold nanoparticles: A highly active bifunctional electrocatalyst for rechargeable lithium-air batteries. *J. Am. Chem. Soc.* **2010**, *132*, 12170–12171.
56. McCloskey, B.D.; Scheffler, R.; Speidel, A.; Bethune, D.S.; Shelby, R.M.; Luntz, A.C. On the efficacy of electrocatalysis in nonaqueous Li-O₂ batteries. *J. Am. Chem. Soc.* **2011**, *133*, 18038–18041.
57. Hassoun, J.; Jung, H.-G.; Lee, D.-J.; Park, J.-B.; Amine, K.; Sun, Y.-K.; Scrosati, B. A metal-free, lithium-ion oxygen battery: A step forward to safety in lithium-air batteries. *Nano Lett.* **2012**, *12*, 5775–5779.
58. Jang, B.Z.; Liu, C.; Neff, D.; Yu, Z.; Wang, M.C.; Xiong, W.; Zhamu, A. Graphene surface-enabled lithium ion-exchanging cells: Next-generation high-power energy storage devices. *Nano Lett.* **2011**, *11*, 3785–3791.
59. Jung, H.-G.; Kim, H.-S.; Park, J.-B.; Oh, I.-H.; Hassoun, J.; Yoon, C.S.; Scrosati, B.; Sun, Y.-K. A transmission electron microscopy study of the electrochemical process of lithium-oxygen cells. *Nano Lett.* **2012**, *12*, 4333–4335.
60. Jung, H.-G.; Hassoun, J.; Park, J.-B.; Sun, Y.-K.; Scrosati, B. An improved high-performance lithium-air battery. *Nat. Chem.* **2012**, *4*, 579–585.
61. Oh, S.H.; Black, R.; Pomerantseva, E.; Lee, J.-H.; Nazar, L.F. Synthesis of a metallic mesoporous pyrochlore as a catalyst for lithium-O₂ batteries. *Nat. Chem.* **2012**, *4*, 1004–1010.
62. Peng, Z.; Freunberger, S.A.; Chen, Y.; Bruce, P.G. A reversible and higher-rate Li-O₂ battery. *Science* **2012**, *337*, 563–566.
63. Abraham, K.M.; Jiang, Z. A polymer electrolyte-based rechargeable lithium/oxygen battery. *J. Electrochem. Soc.* **1996**, *143*, 1–5.
64. McCloskey, B.D.; Speidel, A.; Scheffler, R.; Miller, D.C.; Viswanathan, V.; Hummelshoj, J.S.; Norskov, J.K.; Luntz, A.C. Twin problems of interfacial carbonate formation in nonaqueous Li-O₂ batteries. *J. Phys. Chem. Lett.* **2012**, *3*, 997–1001.
65. McCloskey, B.D.; Bethune, D.S.; Shelby, R.M.; Girishkumar, G.; Luntz, A.C. Solvents' critical role in nonaqueous lithium-oxygen battery electrochemistry. *J. Phys. Chem. Lett.* **2011**, *2*, 1161–1166.
66. Wang, Y.F.; Zheng, D.; Yang, X.Q.; Qu, D.Y. High rate oxygen reduction in non-aqueous electrolyte with the addition of perfluorinated additives. *Energy Environ. Sci.* **2011**, *4*, 3697–3702.
67. Freunberger, S.A.; Chen, Y.; Peng, Z.; Griffin, J.M.; Hardwick, L.J.; Barde, F.; Novak, P.; Bruce, P.G. Reactions in the rechargeable lithium-O₂ battery with alkyl carbonate electrolytes. *J. Am. Chem. Soc.* **2011**, *133*, 8040–8047.
68. Bryantsev, V.S.; Blanco, M. Computational study of the mechanisms of superoxide-induced decomposition of organic carbonate-based electrolytes. *J. Phys. Chem. Lett.* **2011**, *2*, 379–383.
69. Hummelshoj, J.S.; Blomqvist, J.; Datta, S.; Vegge, T.; Rossmeisl, J.; Thygesen, K.S.; Luntz, A.C.; Jacobsen, K.W.; Norskov, J.K. Communications: Elementary oxygen electrode reactions in the aprotic Li-air battery. *J. Chem. Phys.* **2010**, *132*, 071101:1–071101:4.
70. Garcia-Lastra, J.M.; Bass, J.D.; Thygesen, K.S. Communication: Strong excitonic and vibronic effects determine the optical properties of Li₂O₂. *J. Chem. Phys.* **2011**, *135*, 121101:1–121101:4.

71. Ong, S.P.; Mo, Y.; Ceder, G. Low hole polaron migration barrier in lithium peroxide. *Phys. Rev. B* **2012**, *85*, doi:10.1103/PhysRevB.85.081105.
72. Chen, J.; Hummelshoj, J.S.; Thygesen, K.S.; Myrdal, J.S.G.; Nørskov, J.K.; Vegge, T. The role of transition metal interfaces on the electronic transport in lithium-air batteries. *Catal. Today* **2011**, *165*, 2–9.
73. Mitchell, R.R.; Gallant, B.M.; Thompson, C.V.; Shao-Horn, Y. All-carbon-nanofiber electrodes for high-energy rechargeable Li-O₂ batteries. *Energy Environ. Sci.* **2011**, *4*, 2952–2958.
74. Fehér, F.; Wilucki, I.V.; Dost, G. Beiträge zur Kenntnis des Wasserstoffperoxyds und seiner Derivate, VII. Mitteil.: Über die Kristallstruktur des Lithiumperoxyds, Li₂O₂, (in German). *Chem. Ber.* **1953**, *86*, 1429–1437.
75. Föppl, Z. Die Kristallstrukturen der Alkaliperoxyde, (in Danish). *Anorg. Allg. Chem.* **1957**, *291*, 12–50.
76. Xiao, J.; Wang, D.; Xu, W.; Wang, D.; Williford, R.E.; Liu, J.; Zhang, J.-G. Optimization of air electrode for Li/air batteries. *J. Electrochem. Soc.* **2010**, *157*, A487–A492.
77. Zhang, S.S.; Foster, D.; Read, J. Discharge characteristic of a non-aqueous electrolyte Li-O₂ battery. *J. Power Sources* **2010**, *195*, 1235–1240.
78. Debart, A.; Paterson, A.J.; Bao, J.; Bruce, P.G. α -MnO₂ nanowires: A catalyst for the O₂ electrode in rechargeable lithium batteries. *Angew. Chem. Int. Ed.* **2008**, *47*, 4521–4524.
79. Elam, J.W.; Routkevitch, D.; Mardilovich, P.P.; George, S.M. Conformal coating on ultrahigh-aspect-ratio nanopores of anodic alumina by atomic layer deposition. *Chem. Mater.* **2003**, *15*, 3507–3517.
80. Shin, H.; Jeong, D.-K.; Lee, J.; Sung, M.M.; Kim, J. Formation of TiO₂ and ZrO₂ nanotubes using atomic layer deposition with ultraprecise control of the wall thickness. *Adv. Mater.* **2004**, *16*, 1197–1200.
81. Chen, P.; Mitsui, T.; Farmer, D.B.; Golovchenko, J.; Gordon, R.G.; Branton, D. Atomic layer deposition to fine-tune the surface properties and diameters of fabricated nanopores. *Nano Lett.* **2004**, *4*, 1333–1337.
82. Sun, Y.G.; Choi, W.M.; Jiang, H.Q.; Huang, Y.G.Y.; Rogers, J.A. Controlled buckling of semiconductor nanoribbons for stretchable electronics. *Nat. Nanotechnol.* **2006**, *1*, 201–207.